

CHAPTER NINE: EROSION TESTS ON NEW ORLEANS LEVEE SAMPLES

9.1 Erodibility: A Definition

Erodibility is a term often used in scour and erosion studies. Erodibility may be thought of as one number which characterizes the rate at which a soil is eroded by the flowing water. With this concept erosion resistant soils would have a low erodibility index and erosion sensitive soils would have a high erodibility index. This concept is not appropriate; indeed the water velocity can vary drastically from say 0 m/s to 5 m/s or more and therefore the erodibility is not a single number but a relationship between the velocity applied and the corresponding erosion rate experienced by the soils. While this is an improved definition of erodibility, it still presents some problems because water velocity is a vector quantity which varies everywhere in the flow and is theoretically zero at the soil water interface. It is much preferable to quantify the action of the water on the soil by using the shear stress applied by the water on the soil at the water-soil interface. Erodibility is therefore defined here as the relationship between the erosion rate \dot{z} and the hydraulic shear stress applied τ (Figure 9.1). This relationship is called the erosion function $\dot{z}(\tau)$. The erodibility of a soil or a rock is represented by the erosion function of that soil or rock. This erosion function can be obtained by using a laboratory device called the EFA (Erosion Function Apparatus) and described later.

9.2 Erosion Process

Soils are eroded particle by particle in the case of coarse-grained soils (cohesionless soils). In the case of fine-grained soils (cohesive soils), erosion can take place particle by particle but also block of particles by block of particles. The boundaries of these blocks are formed naturally in the soil matrix by micro-fissures due to various phenomena including compression and extension.

The resistance to erosion is influenced by the weight of the particles for coarse grained soils and by a combination of weight and electromagnetic and electrostatic inter-particle forces for fine grained soils. Observations at the soil water interface on slow motion videotapes indicates that the removal of particle or blocks of particles is by a combination of rolling and plucking action of the water on the soil.

9.3 Velocity vs. Shear Stress

The scour process is highly dependent on the shear stress developed by the flowing water at the soil-water interface. Indeed, at that interface the flow is tangential to the soil surface regardless of the flow condition above it; very little water if any flows perpendicular to the interface. The water velocity in the river is in the range of 0.1 to 3 m/s, whereas the bed shear stress is in the range of 1 to 50 N/m² (Figure 9.2) and increases with the square of the water velocity. The magnitude of this shear stress is a very small fraction of the undrained shear strength of clays used in foundation engineering (Figure 9.3).

It is interesting to note that such small shear stresses are able to scour rocks to a depth of 1,600 m, as in the case for the Grand Canyon over the last 20 million years at an average scour rate of 9.1×10^{-6} mm/hr. This leads one to think that even small shear stresses if applied cyclically by the turbulent nature of the flow can overcome, after a sufficient number of cycles, the crystalline bonds in a rock and the electromagnetic bonds in a clay. This also leads one to think that there is no cyclic stress threshold, but that any stress is associated with a number of cycles to failure. (Gravity bonds seem to be an exception to this postulate, because it appears that gravity bonds cannot be weakened by cyclic loading.) This postulate contradicts the critical shear stress concept discussed later.

The profile of the water velocity versus depth in the flow (Figure 9.4) indicates a maximum velocity at the free surface and a zero velocity at the bottom of the flow. This zero velocity boundary is due to the fact that the water does not flow below the flow bottom. While the velocity is zero at the bottom, the shear stress is maximum because the shear stress is proportional to the slope of the velocity profile versus depth. This is explained in Figure 9.4. One can think of the water element in contact with the bottom as a simple shear test on water. Since water is a Newtonian fluid, the shear stress that it develops is proportional to the rate at which it is sheared. This governs the equation in Figure 9.4.

9.4 Erosion Threshold and Erosion Categories

The critical velocity is the velocity at which the soil starts to erode. The critical shear stress is the shear stress at which the soil starts to erode (Figures 9.1 and 9.2). Below these values there is no erosion, above these values the soil erodes at a certain rate. This threshold of erosion is very useful in engineering but it is not obvious that such a clear threshold truly exists physically. Indeed a sample of granite, for example, has a very high critical shear stress. Yet common sense tells us that a pebble made of granite and left under a dripping faucet for 20 million years would develop a hole. In this case, the critical shear as we conceive it would not have been reached yet the rock would have been eroded. The reason for the hole in the pebble may be that there is no such thing as a cyclic threshold for materials and that cyclic stresses even very small can destroy any material bonds; it is only a matter of the number of cycles to break the bond. So one has to accept a practical definition of the critical shear stress. The critical shear stress is defined here as the shear stress corresponding to a rate of erosion of 1 mm/hr in the Erosion Function Apparatus. Values of critical shear stresses are shown in Figure 9.2.

If the critical shear stress is exceeded, it becomes important to know how fast the soil is eroding at a given velocity. The relationship between the erosion rate and the velocity or the interface shear stress is a function. In order to quantify this erosion function using a single number, the following scheme is proposed. It consists in placing the erosion function on the erosion chart of Figure 9.5 and deciding what erodibility category fits best for the soil considered. This approach holds promise to use only one number to characterize a function. Work is ongoing to tie a number of soil types into erodibility categories.

9.5 Erodibility of Coarse-Grained Soils

Clean sands and gravels erode particle by particle. This has been observed on slow motion videotapes. Three mechanisms seem to be possible: sliding, rolling, and plucking.

A simple sliding mechanism (Figure 9.6) consists of assuming that the soil particle is a sphere, that the resultant force exerted by the water on the soil particle is a shear force parallel to the eroding surface, and that neighboring particles do not exert forces on the particle being analyzed because they move at the same rate. Electromagnetic and electrostatic forces between particles are neglected because the analysis is done for a sand or a gravel particle. As the velocity increases, the shear stress τ imposed by the water on the particle becomes large enough to overcome the friction between two particles stacked on top of each other, and sliding takes place. The critical shear stress τ_c is the threshold shear stress at which erosion is initiated. Referring to Figure 9.6, horizontal equilibrium leads to (White 1940):

$$\tau_c A_e = W \tan \phi \quad (1)$$

where A_e = effective friction area of the water on the particle; W = submerged weight of the particle; and ϕ = friction angle of the interface between two particles. If the particle is considered to be a sphere, (1) can be rewritten as

$$\tau_c \alpha (\pi D_{50}^2/4) = (\rho_s - \rho_w) g (\pi D_{50}^3/6) \tan \phi \quad (2)$$

$$\text{or} \quad \tau_c = 2 (\rho_s - \rho_w) g D_{50} (\tan \phi)/3\alpha \quad (3)$$

where α = ratio of the effective friction area over the maximum cross section of the spherical particle; D_{50} = mean diameter representative of the soil particle size distribution; ρ_s and ρ_w = mass density of the particles and of water, respectively; and g = acceleration due to gravity. Eq. (3) shows that the critical shear stress is linearly related to the particle diameter. Briaud et al. (1999b) showed experimentally for a sand and a gravel tested in the EFA that an approximate relationship is:

$$\tau_c (\text{N/m}^2) = D_{50} (\text{mm}) \quad (4)$$

Using (3) and (4), and assuming reasonable values for ρ_s , ρ_w , g , and ϕ , leads to a value of α equal to about 6. This value is many times higher than would be expected and shows that the sliding mechanism is not the eroding mechanism, or at least not the only one involved.

A simple rolling mechanism (Figure 9.7) consists of assuming that the soil particle is a sphere, that the resultant force exerted by the water on the soil particle is a shear force parallel to the eroding surface, that neighboring particles do not impede the process, and that rotation takes place around the contact point with the underlying particle. Electromagnetic and electrostatic forces between particles are neglected because the analysis is done for a sand or a gravel particle. At incipient motion and referring to Figure 9.7, moment equilibrium around the contact point O leads (White 1940) to:

$$\tau_c A_e a = W b \quad (5)$$

$$\text{or} \quad \tau_c (\alpha \pi D_{50}^2/4) (D_{50}/2 + D_{50}(\cos\beta)/2) = (\rho_s - \rho_w) g (\pi D_{50}^3/6) (D_{50}(\sin\beta)/2) \quad (6)$$

$$\text{or} \quad \tau_c = 2 ((\rho_s - \rho_w) g D_{50} \sin\beta)/(3\alpha (1 + \cos\beta)) \quad (7)$$

Eq. (7) confirms that τ_c is linearly proportional to D_{50} . For reasonable values of ρ_s , ρ_w , and g , and for $\alpha = 1$, using (4) and (7) leads to β values equal to about $10-12^\circ$, which is indicative of a loose arrangement; indeed, the sand and the gravel tested to obtain Eq. 4 were placed in a very loose condition in the EFA. Therefore it appears that rolling is more reasonable a mechanism than sliding. Equation 7 tends to indicate that, while τ_c is linearly proportional to D_{50} , the proportionality factor may depend on the relative density. The dominant value of the

angle β can be obtained from a contact angle distribution diagram such as the ones shown in Figure 9.8.

A simple plucking mechanism consists of assuming that the particles are cubes with a side a . The water pressure on top of the cube is u_t and the water pressure at the bottom of the cube is u_b . If it is assumed that all particles are plucked up at the same time, the differential pressure between the top and bottom necessary to initiate plucking of the particle or block of particles is:

$$W = (u_b - u_t) a^2 \quad (8)$$

$$\text{or} \quad \rho_s g a = u_b - u_t \quad (9)$$

The differential pressure $u_b - u_t$ is made up of the hydrostatic differential water pressure $(u_b - u_t)_o$ and the differential water pressure created by the flow Δu

$$\text{or} \quad u_b - u_t = (u_b - u_t)_o + \Delta u \quad (10)$$

For a particle with $a = 1$ mm, the hydrostatic differential water pressure $(u_b - u_t)_o$ is 10 N/m^2 . This hydrostatic differential water pressure reduces the weight of the particle to its buoyant weight. The additional differential water pressure necessary to pluck the particle away Δu is 15 N/m^2 . This value of Δu is equivalent to 1.5 mm of water and it is easy to conceive that such a small differential pressure can be developed. It is created dynamically by the water flow including the fluctuations and the turbulence in the water. These pressure fluctuations are very difficult to measure (Einstein and El-Samni, 1949 and Apperley, 1968). These pressure fluctuations can be calculated through advanced numerical simulations.

These simplistic analyses of the sliding, rolling, and plucking mechanisms help to clarify the important factors affecting the incipient motion of coarse grained soils. However, they are not reliable for prediction purposes, and today experiments are favored over theoretical expressions to determine τ_c for example. Shields (1936) ran a series of flume experiments with water flowing over flat beds of sands. He plotted the results of his experiments in a dimensionless form on what is now known as the Shields diagram. This data as well as other data on sand gathered at Texas A&M University are plotted in Figure 9.2 as critical shear stress τ_c versus mean grain size D_{50} . Eq. (4) is shown in Figure 9.2 and seems to fit well for sands. Shields did not perform any experiments on silts and clays. The data developed for silts and clays at Texas A&M University show that Eq.(4) is not applicable to fine grained soils and that D_{50} is not a good predictor of τ_c for those types of soils.

There seems to be consensus in using the shear stress applied by the water to the soil at the soil water interface as the major parameter causing erosion. It is likely that the hydraulic normal stress or pressure created by the water at that interface also contributes to the process.. Nevertheless, the use of the shear stress only has remained common practice and the role of the normal stress that generates bursts of uplift forces during turbulent flow has yet to be included in common approaches to scour.

9.6 Erodibility of Fine-Grained Soils

In the case of silts and clays, other forces come into play besides the weight of the particles; these are the electrostatic and Van der Waals forces. Figure 9.10 and 9.11 show cartoons of the forces and pressures acting on the soil particle in the general case. The water

pressure u_w surrounds the particle if the soil is saturated. The contact forces f_{ci} exist at the contact point and have normal as well as shear components. The electrostatic and Van der Waals forces f_{ei} are also shown on the figure. Figure 9.10 refers to the case where the water is not moving. In this case the water pressure is smaller on the top of the particle than on the bottom of the particle but the difference is not significant. This difference is equal to the hydrostatic pressure difference due to the height of the particle and creates the buoyancy of the soil particle. In Figure 9.11, the water is moving and the difference between the top and bottom water pressure has increased. Note that the water pressure u_w and therefore the uplift force on the particle is a function of time t and fluctuates during the flow. The cartoon shows a situation where the water pressure may be such that the particle weight is overcome.

The electrostatic forces are likely to be repulsive because clay particles are negatively charged. Van der Waals forces are relatively weak electromagnetic forces that attract molecules to each other (Mitchell 1993); although electrically neutral, the molecules form dipoles that attract each other like magnets. The Van der Waals forces are the forces that keep H_2O molecules together in water. The magnitude of these Van der Waals forces can be estimated by (after Black et al. 1960):

$$f(N/m^2) = 10^{-28} / d(m)^4 \quad (11)$$

where $d(m)$ = distance in m between soil particles; and f = attraction force in N/m^2 . By multiplying f by the particle surface area, one can obtain the inter-particle force. Table 9.1 shows the value of these forces for a sand and a clay particle.

In both cases the soil particle was assumed to be spherical and the distance between particles was taken equal to the particle diameter. While such an evaluation of the Van der Waals force can only be considered as a crude estimate, the following observations regarding the numbers in Table 9.1 are interesting. First, the ratio between the weight and size of the sand particle and the clay particle are similar to the ratio between the weight and size of a Boeing 747 and a postage stamp; therefore, if the critical shear stress is proportional to the particle weight, the critical shear stress for clays should be practically zero. Second, the ratio between the Van der Waals force and the weight of the sand particle indicates that the Van der Waals force is truly negligible for sands. Third, the same ratio for the clay particle, while 10^{17} times larger than for sand, also indicates that the Van der Waals forces are negligible compared with the weight of the clay particle. This would lead one to think that the critical shear stress, τ_c , is essentially zero for clays. Note that the electrostatic forces have not been calculated here but since they are predominantly repulsive they would decrease, if anything, the attraction due to the Van der Waals forces. Other phenomena give cohesion to clays; they include water meniscus forces, such as those developing when a clay dries, and diagenetic bonds due to aging, such as those developing when a clay turns into rock under pressure over geologic time. Because of the number and complexity of these bonds, it is very difficult to predict τ_c for clays empirically on the basis of a few index properties. Several researchers however have proposed empirical equations for τ_c in clays, such as Dunn (1959) and Lyle and Smerdon (1965).

One problem associated with measuring τ_c is determining the initiation of scour. When the particles are visible to the naked eye, it is simple to detect when the first particle is scoured away. For clays this is not the case, and various investigators define the initiation of

scour through different means; these vary from “when the water becomes muddy” to extrapolation of the scour rate versus shear stress curve back to zero scour rate. Table 9.2 shows a variety of measured τ_c values. The lack of precise definition for the initiation of scour may be in part responsible for the wide range of values.

Beyond the critical shear stress, a certain scour rate z' (mm/hr) is established. This scour rate is rapid in sand, slow in clay, and extremely slow in rock. The example of the Grand Canyon rock cited earlier leads to a value of z' equal to 9.1×10^{-6} mm/hr, whereas fine sands erode at rates of 10^4 mm/hr as measured in the EFA. Clays scour at intermediate rates with common values in the range of 1 to 1,000 mm/hr. The high scour rate in sand exists because once gravity is overcome, no other force slows the scour process down. The very low scour rate in rock exists probably because it takes a large number of shear-stress cycles imposed by the turbulent nature of the flow to overcome the very strong crystalline bonds binding the rock together. Note that rock scour can also occur at larger rates if the rock is fractured and the water flow provides very high velocities as in the case of the downstream end of high dam spillways. The low scour rate in clays is probably associated with the fact that it takes a large number of shear stress cycles to overcome the electromagnetic bonds created by the Van der Waals forces between clay particles. Even though these bonds are relatively weak, as discussed previously, they are sufficient to slow the scour process significantly. The scour rate z' versus shear stress τ_c curve (Figure 9.1) is used to quantify the scour rate of a soil as a function of the flow. Several researchers have measured the rate of erosion in cohesive soils; most have proposed a straight line variation (Ariathurai and Arulanandan, 1978), while some have found S shape curves (Christensen, 1965). Some of the rates quoted in the literature are given in Table 9.3.

Some of the factors influencing the erodibility of fine grained soils are listed in Table 9.4. Although there are sometimes conflicting findings, the influence of various factors on cohesive soil erodibility is shown in Table 9.4 when possible.

The critical shear stress of coarse grained soils is tied to the size of the particles and usually ranges from 0.1 N/m^2 to 5 N/m^2 . The rate of erosion of coarse grained soils above the critical shear stress increases rapidly and can reach tens of thousands of millimeters per hour. The most erodible soils are fine sands and silts with mean grain sizes in the 0.1 mm range (Figure 9.2). The critical shear stress of fine grained soils is not tied to the particle size but rather to a number of factors as listed in Table 9.4. The critical shear stress of fine grained soils however varies within the same range as coarse grained soils (0.1 N/m^2 to 5 N/m^2) for the most common cases. One major difference between coarse grained and fine grained soils is the rate of erosion beyond the critical shear stress. In fine grained soils (often called cohesive soils), this rate increases slowly and is measured in millimeters per hour. This slow rate makes it advantageous to consider that erosion problems are time dependent and to find ways to accumulate the effect of the complete velocity history rather than to consider a design flood alone.

9.7 Erodibility and Correlation to Soil Properties

There is a critical shear stress τ_c below which no erosion occurs and above which erosion starts. This concept while practically convenient may not be theoretically simple.

Indeed, as seen on Figure 9.1, there is no obvious value for the critical shear stress. The critical shear stress is arbitrarily defined as the shear stress which corresponds to an erosion rate of 1 mm/hr. The critical shear stress is associated with the critical velocity v_c . One can also define the initial slope $S_i = (dz/dt)_i$ at the origin of the erosion function. Both τ_c and S_i are parameters which help describe the erosion function and therefore the erodibility of a material.

In coarse grained soils (sands and gravels), the critical shear stress has been empirically related to the mean grain size D_{50} (Briaud et al., 2001a).

$$\tau_c \text{ (N/m}^2\text{)} = D_{50} \text{ (mm)} \quad (12)$$

For such soils, the erosion rate beyond the critical shear stress is very rapid and one flood is long enough to reach the maximum scour depth. Therefore there is a need to be able to predict the critical shear stress to know if there will be scour or no scour but there is little need to define the erosion function beyond that point because the erosion rate is not sufficiently slow to warrant a time dependent analysis.

In fine grained soils (silts, clays) and rocks, equation 12 is not applicable (Figure 9.2) and the erosion rate is sufficiently slow that a time rate analysis is warranted. Therefore it is necessary to obtain the complete erosion function. An attempt was made to correlate those parameters, τ_c and S_i , to common soil properties in hope that simple equations could be developed for everyday use. The process consisted of measuring the erosion function on one hand and common soil properties on the other (water content, unit weight, plasticity index, percent passing sieve no. 200, undrained shear strength). This led to a database of 91 EFA tests (Table 9.5) which was used to perform regression analyses and obtain correlation equations (Figure 9.12 to 9.15). All attempts failed to reach a reasonable R^2 value.

The fact that no relationship could be found between the critical shear stress or the initial slope of the erosion function on one hand and common soil properties on the other seems to be at odds with the accepted idea that different cohesive soils erode at different rates. Indeed if different clays erode at different rates then the erosion function and therefore its parameters should be functions of the soils properties. The likely explanation is that there is a relationship between erodibility and soils properties but that this relationship is quite complicated, involves advanced soil properties, and has not been found. Instead, it was found much easier to develop an apparatus which could measure the erosion function on any sample of cohesive soil from a site. This apparatus was called the Erosion Function Apparatus or EFA.

9.8 The EFA: Erosion Function Apparatus

The EFA (Briaud et al. 1999, Briaud et al., 2001a) was conceived by Dr. Briaud in 1991, designed in 1992, and built in 1993 (Figure 9.16). The sample of soil, fine-grained or not, is taken in the field by pushing an ASTM standard Shelby tube with a 76.2 mm outside diameter (ASTM D1587). One end of the Shelby tube full of soil is placed through a circular opening in the bottom of a rectangular cross section pipe. A snug fit and an O-ring establish a leak proof connection. The cross section of the rectangular pipe is 101.6 mm by 50.8 mm. The pipe is 1.22 m long and has a flow straightener at one end. The water is driven through the pipe by a pump. A valve regulates the flow and a flow meter is used to measure the flow rate.

The range of mean flow velocities is 0.1 m/s to 6 m/s. The end of the Shelby tube is held flush with the bottom of the rectangular pipe. A piston at the bottom end of the sampling tube pushes the soil until it protrudes 1 mm into the rectangular pipe at the other end. This 1 mm protrusion of soil is eroded by the water flowing over it.

9.8.1 EFA test procedure

The procedure for the EFA test consists of

1. Place the sample in the EFA, fill the pipe with water, and wait one hour.
2. Set the velocity to 0.3 m/s.
3. Push the soil 1 mm into the flow.
4. Record how much time it takes for the 1 mm soil to erode (visual inspection)
5. When the 1 mm of soil is eroded or after 30 minutes of flow whichever comes first, increase the velocity to 0.6 m/s and bring the soil back to a 1 mm protrusion.
6. Repeat step 4.
7. Then repeat steps 5 and 6 for velocities equal to 1.0 m/s, 1.5 m/s, 2 m/s, 3 m/s, 4.5 m/s, and 6 m/s. The choice of velocity can be adjusted as needed.

9.8.2 EFA test data reduction

The test result consists of the erosion rate dz/dt versus shear stress τ curve (Figure 9.1, and 16). For each flow velocity v , the erosion rate dz/dt (mm/hr) is simply obtained by dividing the length of sample eroded by the time required to do so.

$$dz/dt = h/t \quad (13)$$

Where h is the length of soil sample eroded in a time t . The length h is 1 mm and the time t is the time required for the sample to be eroded flush with the bottom of the pipe (visual inspection through a Plexiglas window). After several attempts at measuring the shear stress τ in the apparatus it was found that the best way to obtain τ was by using the Moody Chart (Moody, 1944) for pipe flows.

$$\tau = f \rho v^2/8 \quad (14)$$

Where τ is the shear stress on the wall of the pipe, f is the friction factor obtained from Moody Chart (Figure 9.17), ρ is the mass density of water (1000 kg/m³), and v is the mean flow velocity in the pipe. The friction factor f is a function of the pipe Reynolds number Re and the pipe roughness ϵ/D . The Reynolds number is $Re = vD/\nu$ where D is the pipe diameter and ν is the kinematic viscosity of water (10⁻⁶ m²/s at 20°C). Since the pipe in the EFA has a rectangular cross section, D is taken as the hydraulic diameter $D = 4A/P$ (Munson et al., 1990) where A is the cross sectional flow area, P is the wetted perimeter, and the factor 4 is used to ensure that the hydraulic diameter is equal to the diameter for a circular pipe. For a rectangular cross section pipe:

$$D = 2ab/(a + b) \quad (15)$$

Where a and b are the dimensions of the sides of the rectangle. The relative roughness ϵ/D is the ratio of the average height of the roughness elements on the pipe surface over the pipe diameter D . The average height of the roughness elements ϵ is taken equal to $0.5D_{50}$ where D_{50} is the mean grain size for the soil. The factor 0.5 is used because it is assumed that the top half of the particle protrudes into the flow while the bottom half is buried into the soil

mass. During the test, it is possible for the soil surface to become rougher than just $0.5 D_{50}$; this occurs when the soil erodes block by block rather than particle by particle. In this case the value used for ε is estimated by the operator on the basis of inspection through the test window. Typical EFA test results are shown on Figure 9.1 for sand and then clay.

9.9 Some Existing Knowledge on Levee Erosion

9.9.1 Current Considerations in Design

The US Army Corps of Engineers' design manual (USACE, 2000) outlines the steps followed in the design and construction of levees (Table 9.6). The procedure does not include an evaluation of the erodibility of the soils used for the levees. A more in-depth discussion of design requirements is presented in Chapter 10.

9.9.2 Failure Mechanism

Flowing water exerts a tractive shear stress along the soil-water interface. The erosion process begins when this tractive shear stress exceeds the resistive force of the backslope soil (AlQaser, 1991). Hanson et al. (2003) describe four stages of erosion during the overtopping of cohesive embankments (Figure 9.18):

- Stage I:** Minor headcut movement up to the downstream embankment crest; surface erosion occurs.
- Stage II:** Headcut progresses from the downstream embankment crest to the upstream embankment crest.
- Stage III:** The crest lowers and breach formation begins as the headcut continues to migrate upstream of the embankment crest.
- Stage IV:** Erosion of the breach opening has progressed to near the base of the upstream toe of the embankment; driven by erosion of the sidewalls and development of an overhang, resulting in episodic mass failures and breach widening (Hunt et al., 2004).

Erosion typically occurs adjacent to some change or interruption in the flow pattern (Ralston, 1987). The turbulence associated with the flow disturbance breaks down the protective boundary laminar flow layer. This leads to the occurrence of full hydraulic stress intensity as well as rapid stress reversals, greatly increasing the erosion rate.

Gradually varied flow also leads to non-uniform erosion along the backslope producing overfalls. The overfall will advance progressively headward as long as the remaining embankment material can support the dam crest and upstream slope (Figure 9.19). The base of the overfall will deepen and widen.

As the eroding vertical overfall face advances headward, the overflow crest elevation will lower, cutting into the adverse grade of the upstream slope. This erosion pattern will continue and progress until the flow pattern changes into a free surface flow (Figure 9.20, AlQaser, Ruff, 1993). Headward advance of the overfalls is due to a combination of the following:

- 1) Insufficient soil strength to stand vertically due to the height of the face, stress relief cracking, and induced hydrostatic pressure in the cracks
- 2) Loss of foundation support for the vertical face due to the waterfall plunging effect and its associated lateral and vertical scour. As the vertical overfall gets higher, impact energy of the water fall increases, the rate of erosion increases and the scour hole becomes larger. The supporting foundation of the overfall face and sidewalls is thus removed.

The erosion pattern of embankments using non-cohesive soil is affected by the existence and location of a cohesive soil zone. For purely non-cohesive embankments, the erosion occurs on a uniform, but gradually flattening gradient. This erosion pattern can be modeled using the theory of tractive stress. The breach development is consistent with the principle of minimum rate of energy dissipation for streams (Coleman et al., 2002). Breaches, like streams, tend to alter their geometry in order to produce a minimum rate of energy dissipation. When the embankment includes a zone of cohesive soil, the overfall development will be retarded. If the zone is symmetrical, erosion will behave similar to that of a cohesive soil embankment. If the zone is an upstream sloping section, the overflow crest will degrade. This is due to undermining of the downstream non-cohesive zone. Portions of the overhanging cohesive zone will subsequently break off as the allowable bending moment is exceeded.

9.9.3 Numerical modeling

Erosion computer models are used to describe and quantify the complexities associated with an embankment breach. OVERFALL, a computer program developed by AlQaser (1991), predicts the heights and numbers of overfalls along the backslope of an overtopped embankment. Key features of breaches can also be reproduced with SIMBA, or SIMplified Breach Analysis (Temple et al., 2005). This model has been verified against embankment breach tests. Presently, SIMBA is only capable of addressing homogeneous embankment conditions. Future work will allow for applications to non-homogeneous field conditions, though.

Breach and discharge characteristics can be modeled and predicted with BREACH (Fread, 1988). BREACH allows for predictions of the size, shape, and time of formation of an earthen dam breach. A breach outflow hydrograph is also provided from the analysis. The extent of the enlargement, the peak outflow, and the time to peak flow are determined by the internal friction angle and the cohesive strength of the embankment soil. The BREACH model was verified by comparing the results of the model and several overtopping failure tests. These tests were conducted in different countries at varying scales with different homogeneous materials and construction practices. A summary of dam break numerical models that can be used for gradual failure is shown in Table 9.7.

9.9.4 Laboratory Tests

Nairn (1986) conducted two-dimensional flume tests to study cohesive shore erosion. Tests were conducted on artificial clay, composed of a bentonite-silt mixture, with and without an overlying veneer of sand. Surprisingly, the flume tests with sand did not lead to failure as the sand acted as an armor over the clay. Tests without sand, however, produced

responses close to those observed in the field. Table 9.8 displays the erosion rate results for the flume tests conducted by Nairn. Dodge (1988) also conducted laboratory flume tests to study erosion of a clayey sand (Figure 9.21). The results of the tests were not verified with field observations; they serve to provide a qualitative assessment of erosion.

AlQaser (1991) performed two laboratory tests to study progressive failure of an overtopped embankment (Figure 9.22). Both tests had the same design, but differed in the percent of sand in the soil. The first sample consisted of 80% clay and 20% sand. The other had 50% clay and 50% sand. Results show that the presence of more clay in the soil mixture leads to a greater vertical overfall height. The soil with more sand in the mixture, however, resulted in more horizontal overfall regression. It is concluded, therefore, that the physical and the geometrical properties of the embankment affect the number and heights of the developed overfalls.

9.9.5 Field Tests

Hanson, Cook, and Hahn (2001) describe preliminary evaluation of the headcut migration rates during overtopping and breaching tests on large-scale models. The headcut advance threshold was evaluated based on an energy dissipation term:

$$E = q\gamma_w H \quad (16)$$

Where q = unit discharge, γ_w = unit weight of water, and H = Headcut height. The headcut migration rates for each test section were evaluated and compared to measured soil properties, such as erodibility and soil strength. The results show that as soil strength decreases, the headcut migration rate increases (Figure 9.23).

The breaching of non-cohesive homogeneous embankments under constant-reservoir levels was studied using flume tests (Figure 9.24) by Coleman et al. (2002). This experiment simulated the failure of an embankment restricting a very large upstream reservoir. A small V breach was initiated and grew as erosion took place. A wide range of uniform non-cohesive soils were tested. The quantitative findings of these tests have not been verified by the results from large scale embankments.

It was found from the flume tests conducted by Coleman et al. (2002) that erosion progresses from primarily vertical to lateral in nature. This occurs as the breach channel invert approaches the foundation level. The channel invert slope will flatten as it rotates about a fixed pivot point, X_p , on the embankment (Figure 9.25).

The location of this pivot point is a function of the embankment sediment size. In plan view, the breach channel develops into an hourglass (or Venturi) shape (Figure 9.26). The curvature of the channel increases with time until the embankment foundation impedes the vertical erosion of the breach. This leads to an increase in the rounding of the approach and exit channels.

After the preliminary studies of 2001, Hanson, Cook, et al. (2003) performed a second study of the headcut migration and erosion widening rates during overtopping. They used large-scale models and three soils including two non-plastic (SM) silty sand materials and a

(CL) lean clay. The width of the breach during testing was evaluated using photographic measurements of the model embankment (Figure 9.27). Details of the testing indicated that headcut erosion was an important erosion process in the failure of cohesive embankments. It can influence the breach initiation time, breach formation time, breach width, peak discharge, and the overall outflow hydrograph.

The headcut migration rates (Figure 9.28), as well as the erosion widening rates (Figure 9.29), show a direct correlation to the compaction water content. The rate of breach widening was found by taking the linear regression of the breach width measurement from left bank to right bank versus time (Figure 9.30). The observed breach widths during testing were equal to two to five times the dam height. Figure 9.31 indicates that the head cutting rate for stages II and III of the erosion process is larger than the widening rate at the beginning but becomes approximately equal to it towards the end of the breaching process.

9.9.6 Factors Influencing Resistance to Overtopping

For a given soil, Hanson et al. (2003) show that erodibility correlates well with compaction water content, energy, density, and texture. By contrast, Cao et al. (2002) using a large data base found no relationship between common soil properties and the erodibility of cohesive soils. Dodge (1988, Figure 9.32) gave some trends of erodibility for cohesive soils using the plasticity chart. The FHWA (Chen, Cotton, 1988) also presents a plot of permissible shear stresses for cohesive soils based on the plasticity index (Figure 9.33).

Choliaras et al. (2003) concludes that the main measure of erosivity of overland flow is shear stress flow. He states that the increase of erosion rate is linear with shear stress of flow. He adds that for low values of surface shear stress, the erodibility of a soil decreases with increasing soil strength while for high values of surface shear stress, the erodibility of the soil increases with increasing surface strength.

According to Fread (1988), the growth of a breach is dependent on the soil properties of the dam. Unit weight, friction angle, and cohesive strength are shown to influence the size, shape, and time of formation of a breach. The amount of grass cover on the dam is also a factor in breach formation.

The results of the research performed by AlQaser (1991) point to poor compaction as a source of breaching. According to model tests conducted by Dodge (1988), the volume of scour produced during flow can be decreased by increasing the compaction of the soil.

Similarly, for clay soils, an increase in density reduces erodibility (Choliaras et al., 2003). For silty and sandy soils, the density or compaction of the soil does not significantly influence erodibility.

1953 Levee (Dike) failures in Netherlands

The Netherlands is a country of 8.5 Million people and 26% of them live below mean sea level protected by levees (Gerritsen, 2006). The following is a summary of an excellent article by Gerritsen in Geo-Strata (2006) which describes the 1953 disaster and the steps taken since

then by the Netherlands. Prior to 1953 the dikes were at a height equal to the maximum recorded water level plus 0.5 m. The height of some of the levees had been increased by constructing concrete walls along the levee crest. During World War II, the levees were used as a defense system and many holes were dug to that effect. After the war, the damage done to the levees was not adequately repaired.

On January 31, 1953, a North Sea storm combined with high tide and raised the water level to unprecedented height and 150 levee breaches occurred. During that storm, 1836 people died, 100,000 people evacuated, tens of thousands of livestock perished, and 136,500 hectares were inundated. The levee breaches were attributed to sustained wave overtopping. The land side of the levees was typically at a steeper slope (1v to 1.5h or 1v to 2h) than the sea side (1v to 3h or more). The failure process initiated from the land side and progressed backward towards the sea side. One sign of imminent failure was a longitudinal crack forming along the crest of the levee which was quickly filled by the rushing water.

On February 18, 1953, a committee was formed called the Delta Committee with the task of ensuring that such a disaster would not happen again. The committee chose to solve the problem not by increasing the height of the levees but rather by recommending the Delta Plan. This plan consisted of closing the shoreline completely through a series of permanent barriers to be built over a 20 year period. In 1975, due to political pressures from the fishing industry, the barriers were changed from complete damming to moveable storm surge barriers to be closed only in the event where a North Sea storm would coincide with a high tide.

The Netherlands now requires that the flood protection systems satisfy the following

- Be able to resist a storm surge with a probability of occurrence of 1/10,000 for the Province of Holland;
- Be able to resist a storm surge with a probability of occurrence of 1/4000 for less populated coastal areas; and
- Be reviewed and evaluated every 5 years with associated recommendations to be constructed in the following 5 years.

9.9.7 Influence of Grass Cover on Surface Erosion

Grass makes a difference in the resistance to surface erosion (Figure 9.34). The physical vegetative coverage on slopes provides increased resistance through underground soil reinforcement and surface protection (Li and Eddleman, 2002). Root systems aid slope stabilization through soil-root interaction. The mechanics of root-reinforcement are similar to the basic mechanics of engineering reinforced-earth systems (Coppin and Richards, 1990). The vegetation root growth reinforces the upper soil layers increasing the soil shear strength by over 33 % (Bhandari et al., 1998). Many researchers have developed theoretical models of root-reinforced soils, including Gray and Leiser (1982), Greenway (1987), Coppin and Richards (1990), Styczen and Morgan (1995), and Wu (1995). In general, the vegetative methods for surface erosion control include two types: herbaceous and woody. They all have the following four mechanisms in controlling surface erosion (Gray 1974; Greenway, 1987; Coppin and Richards, 1990):

1. Restraint: The root system binds the soil particles. The foliage residues restrain soil particle detachment via shallow, dense root systems, consequently reducing sediment transport.
2. Retardation: The foliage and stems increase the surface roughness and slow surface runoff.
3. Interception: The foliage and plant residues absorb the rainfall energy by intercepting the raindrops to reduce raindrop impacts.
4. Transpiration: Absorption of soil moisture by plants delays the initiation of saturation and increases shear strength by reducing pore-pressures.

The level of vegetation for protecting the soil depends on the combined effects of roots, stems and foliage (Coppin and Richards, 1990). Woody vegetation installed on slopes and streambanks provides resistance to shallow mass-movement by counterbalancing local instabilities. In order to achieve optimum stabilization, vegetation must establish quickly and solidly. For biotechnical stabilization techniques that only use vegetative materials, the stabilization is vulnerable at the early stage but becomes stronger as the vegetation is established (Li and Eddleman, 2002). For techniques that combine plant and inert materials such as dead wood, rocks or geosynthetics, inert materials support major loads at the early stage. As the vegetation matures, root systems will bind soils, inert materials and vegetation altogether on the slope or streambank, and increase the safety factor of structural protection (Biedenharn et al., 1997).

From the engineering perspective, vegetation's use on slopes or streambanks may not be always ideal. Trees planted on certain parts of levees may have roots undermining the levee stability (USACE, 1999). Greenway (1987), and Coppin and Richards (1990) have analyzed vegetation's engineering functions and determined that its effects are both adverse and beneficial, depending on the circumstances. Therefore, selecting appropriate plant type becomes very critical in such conditions. This can be done by testing at large scale facilities such as the one at Texas A&M University which grows grass and tests it on slopes of various geometries.

Johnston (2003) prepared the chart of Figure 9.35 which gives the allowable shear stress at the interface between the soil and the water flowing on a slope. Different covers are represented including bare soil, grass covered, geosynthetic matting, hard armor. The depth D is the depth of water flowing over the slope S . Note that overall the range of slope covered is fairly shallow.

9.10 Soil and Water Samples Used for Erosion Tests

A total of 11 locations were identified for studying the erosion resistance of the levee soils. Emphasis was placed on levees which were very likely overtopped. These locations are labeled S1 through S15 for Site 1 through Site 15 on Figure 9.36. The samples were taken by pushing a Shelby tube when possible or using a shovel to retrieve soil samples into a plastic bag. For example at Site S1, the drilling rig was driven on top of the levee, stopped at the location of Site 1, a first Shelby tube was pushed with the drilling rig from 0 to 2 ft depth and then a second Shelby tube was pushed from 2 to 4 ft depth in the same hole. These two Shelby tubes belonged to boring B1. The drilling rig advanced a few feet and a second

location B2 at Site S1 was chosen; then two more Shelby tubes were collected in the same way as for B1. This process at Site S1 generated 4 Shelby tube samples designated

- S1-B1-(0-2ft)
- S1-B1-(2-4ft)
- S1-B2-(0-2ft)
- S1-B2-(2-4ft)

Four such Shelby tubes were collected from sites S1, S2, S3, S7, S8, and S12. In a number of cases, Shelby tube samples could not be obtained because access for the drilling rig was not possible (e.g.: access by light boat for the MRGO levee) or pushing a Shelby tube did not yield any sample (clean sands). In these cases, grab samples were collected by using a shovel and filling a plastic bag. The number of bags collected varied from 1 to 4. Plastic bag samples were collected from sites S4, S5, S6, S11, and S15. The total number of sites sampled for erosion testing was therefore 11. These 11 sites generated a total of 23 samples. One of the samples, S8-B1-(2-4ft), exhibited two distinct layers during the EFA tests and therefore lead to two EFA curves. All in all 24 EFA curves were obtained from these 23 samples: 14 performed on Shelby tube samples and 10 on bag samples. The reconstitution of the bag samples in the EFA is discussed later.

Water salinity has an effect on erosion. The salinity of the water was determined by using the soil samples collected at the sites. Samples S11 and S15 were selected because one was on the Lake Pontchartrain side and the other on the Lake Borgne side. The procedure to obtain the consisted of:

1. Dry the soil (about 70 g) in an oven for 12 hr
2. Weigh a quantity of soil, e.g. 10 g and place it in a PE bottle
3. Add deionized (DI) water in the ratio of 2 ml water for one sample and 5 ml water for another sample to each gram of soil
4. Soil: DI water = 10 g: 20 ml or 10g: 50 ml
5. Shake the bottle to thoroughly mix the soil and water
6. Allow the soil to settle for 12 hr
7. Use a pH meter (Orion model 420 A) to measure the pH and a calibrated conductivity meter (Corning model 441) to measure the conductivity of the water.
8. Perform a calibration of the conductivity meter by using known concentrations of salt.
9. Use the conductivity to salinity calibration curve to obtain the salinity of the water created in steps 1 to 7.

Then it becomes necessary to correct the salinity of this water because the amount of water added to the soil for the salinity determination test does not correspond to the amount of water available in the soil pores in its natural state (in the levee). This is done by calculating the amount of water available in the pores of the samples in its natural state. This requires the use of the void ratio and the degree of saturation of the samples calculated using simple phase diagram relationships. The results obtained are shown in Table 9.9.

9.11 Erosion Function Apparatus (EFA) Test Results

9.11.1 Sample Preparation

No special sample preparation was necessary for the samples which were in Shelby tubes. The Shelby tube was simply inserted in the hole on the bottom side of the rectangular cross section pipe of the FEA (described previously).

For bag samples obtained by using a shovel to collect the soil, there was a need to reconstruct the sample. These samples were prepared by re-compacting the soil in the Shelby tube (Figure 9.37). The same process as the one used to prepare a sample for a Proctor compaction test was used. Since it was not known what the compaction level was in the field, two extreme levels of compaction energy were used to recompact the samples. The goal was to bracket the erosion response of the intact soil.

For the high compaction effort (100% of Modified Proctor compaction effort), the sample was compacted in an 18-inch long Shelby tube as follows:

- 1) The total sample height was 6 inches. The sample was compacted in eight layers.
- 2) To form each layer, the soil was poured into the Shelby tube from a height of 1 inch above the top of the tube.
- 3) The soil was compacted using a 10 lb hammer (Modified Proctor hammer) with a drop height of 1.5 feet. Each layer was compacted by 8 hammer blows, i.e. 8 blows/layer.
- 4) This process was repeated until a 6 inch sample was obtained.
- 5) The corresponding compaction energy was equal to the Standard Modified Proctor Compaction energy.

For the low compaction effort (1.63% of Modified Proctor compaction effort), the sample was compacted in an 18-inch long Shelby tube as follows.

1. The total sample height was 6 inches. The sample was compacted in eight layers.
2. To form each layer, the soil was poured into the Shelby tube from a height of 1 inch above the top of the tube.
3. The soil was compacted using a 10 lb hammer (Modified Proctor hammer) with a drop height of 1 inch. Each layer was compacted by 3 hammer blows, i.e. 3 blows/layer.
4. This process was repeated until a 6 inch sample was obtained.
5. The corresponding compaction energy was 1.63% of the Standard Modified Proctor Compaction energy.

9.11.2 Sample EFA Test Results

The procedure described earlier was strictly followed for the EFA tests. The results were prepared in the form of a word file report and an accompanying excel spread sheet detailing the data reduction and associated calculations. The main result of an EFA test is a couple of plots: one is the plot of the erosion rate versus mean velocity in the EFA pipe, the other is the plot of the erosion rate versus shear stress at the interface between the soil and the

water. These two plots are collected in Appendix A for all 24 EFA tests. Figs. 9.38 and 9.39 show two examples of results for a very erodible soil and a very erosion resistant soil.

9.11.3 Summary Erosion Chart

In an effort to give a global rendition of the EFA results, an erosion chart was created. The blank erosion chart has been presented earlier and is reproduced here for convenience (Figure 9.40). This chart allows one to present the erosion curves in a way which categorizes the soils according to one erosion category. Category 1 is very erodible and refers to soils such as clean fine sands. Category 5 is very erosion resistant and refers to soils such as some of the highly compacted and well graded clays.

Figure 9.41 shows the erosion chart populated with the EFA results for all 24 EFA tests. The legend contains the sample/test designation which starts with the site number (Figure 9.36), followed by the boring number, the depth, and letter symbols including SW, TW, LC, HC, and LT. SW stands for Sea Water and means that the water used in the EFA test was salt water at a salinity of approximately 35000 ppm. TW stands for Tap Water and means that the water used in the EFA test was Tap Water at a salinity of approximately 500 ppm. LC stands for Low Compaction, refers to bag samples only, and means that the sample was prepared using 1.6% of Modified Proctor compaction effort. HC stands for High Compaction, refers to bag samples only, and means that the sample was prepared using 100% of Modified Proctor compaction effort. LT stands for Light Tamping and refers to the preparation of some bag samples used in some early tests; it is very similar to the LC preparation.

One of the first observations coming from the summary erosion chart on Figure 9.41 is that the erodibility of the soils obtained from the New Orleans levees varies widely all the way from very high erodibility (Category 1) to very low erodibility (Category 5). This explains in part why some of the overtopped levees failed while other overtopped levees did not. This finding points to the need to evaluate the remaining levees for erodible soils (weak links).

9.11.4 Influence of Compaction on Erodibility

Several of the bag samples were tested at two extreme compaction efforts: 100% Modified Proctor and 1.6% Modified Proctor. Because the low and high compaction samples originated from the same bag of collected soil, it is reasonable to assume that the samples are very similar. The EFA tests results aimed at identifying the influence of the compaction effort are isolated in Figure 9.42. Sample S4 shows a major influence of the compaction effort on the erodibility. Indeed, the low compaction sample is at the border between Category 1 and Category 2 (very high to high erodibility) while the high compaction sample is at the border between Category 4 and Category 5 (very low to low erodibility). However, Samples S15 and S11 do not show much difference between the high compaction and the low compaction.

The index properties of the samples tested are presented in a following section. Sample S4 is a high plasticity silt. It has 90.47 % fines, a plasticity index of 30, and a USCS classification of MH. Sample S11 is a clean uniform sand. It has 0.1 % fines, and a USCS classification of SP. Sample S15 is a silty sand. It has 29.89 % fines, and a USCS classification of SM. These three data points tend to indicate that compaction has a more

significant influence on erodibility for some soils (higher fines content) than for others (lower fine content).

9.11.5 Influence of water salinity on erodibility

Salinity can have an influence on the erodibility of a soil. Several of the samples were tested by using water at two extreme salt concentrations: 35000 ppm to simulate sea water and 500 ppm to simulate water with a very low salt concentration. Because the samples used to check the influence of the water salinity originated from different Shelby tubes at two different depths (0-2 ft and 2-4 ft), it is possible that the samples may have had different erodibility to start with. This may have clouded the influence of the water salinity.

The EFA tests results for the tests aimed at identifying the influence of the water salinity are isolated in Figure 9.43. Conclusions are difficult to draw because the samples may not be from the same soil. One sample (S8-B1) actually was made of two separate layers which had two different erosion functions and lead to two EFA curves for the same Shelby tube.

Nevertheless, the following observations can be made. Samples S12 show that an increase in water salinity increases the resistance to erosion, samples S2 and S8 show no influence, while samples S1 and S7 show a reverse influence of the water salinity. The index properties of the samples tested are presented in a following section. All samples exhibit a high clay content.

9.12 Index Properties of the Samples Tested in the EFA

A set of index property tests were performed on the samples used in the EFA. Some of the tests were performed by Soil Testing Engineering in Baton Rouge, the remainder of the tests were performed at Texas A&M University. Table 9.10 shows a summary of the results as well as the classifications according the Unified Soil Classification System. As can be seen there are no gravels, and mostly sands, silts, and clays.

9.13 Levee Overtopping and Erosion Failure Guideline Chart

In an effort to correlate the results of the EFA erosion tests with the behavior of the levees during overtopping flow, Figure 9.44 was prepared. It seems reasonably sure that the levees at sites S4, S5, S6, and S15 were overtopped and failed. At the same time it seems reasonably sure that the levees at sites S2, and S3 were overtopped and resisted remarkably well. The dark circles on Figure 9.44 correspond to samples taken from levees that were overtopped and failed by erosion while the open circles correspond to samples taken from levees that were overtopped and held up well during that overtopping.

Figure 9.44 shows a definite correlation between the EFA tests results and the behavior of the levees during overtopping. Figure 9.45 was generated from Figure 9.44 as a levee guideline for erosion resistance during overtopping. It is suggested that such EFA erosion tests should be used in the future to predict levee behavior and ensure erosion resistance to overtopping. In addition, this type of testing can be performed on an increased variety of soils, and with varied compaction conditions, to develop generalized relationships

between soil types and soil characteristics, placement and compaction conditions, and resistance to erosion.

9.14 Summary

The results of this pilot study show that we are well able to correlate soil type, soil characteristics, and placement and compaction conditions with embankment performance with regard to erodibility. Moreover, we are also able to perform erodibility tests of specific soils, and for specific placement and compaction conditions, and the results of these tests appear to correlate well with observed field performance with regard to erodibility during levee overtopping in the New Orleans region during hurricane Katrina.

Accordingly, it is clearly possible to identify and avoid the use of materials that can be expected to perform poorly with regard to erosion resistance, and it is feasible to design engineered embankments with a high intrinsic resistance to erosion. That would have been very useful in the New Orleans regional flood protection system, and it appears that avoiding the use of highly erodeable levee embankment fills, and using instead embankment fills engineered to provide improved erosion resistance, would likely have significantly reduced both damages and loss of life in this event.

There is more to be done in further developing and refining these testing procedures and developing generalized correlations between material characteristics and placement conditions vs. erodibility, and also with regard to the development of corollary analysis methods and procedures for making engineering assessments regarding likely rates of erosion, etc., as a function of overtopping intensities, geometries and durations. Nonetheless, it appears that we are able to include resistance to erosion as a deliberately engineered feature of levee embankments. As this adds a potentially important source of additional system resilience, this should be considered in the future for flood protection systems defending large populations at risk.

9.15 References

- AlQaser, G., and Ruff, J. F., (1993), "Progressive failure of an overtopped embankment," Proceedings of the 1993 National Conference on Hydraulic Engineering, Hydraulic Division of ASCE, pp. 1957-1962.
- AlQaser, G.N., (1991), Progressive Failure of an Overtopped Embankment, Ph.D. dissertation, Colorado State University, Fort Collins, CO.
- Apperly, L.W., 1968, "Effect of turbulence on sediment entrainment", PhD dissertation, University of Auckland, Auckland, New Zealand.
- Ariathurai, R., and Arulanandan, K. (1978). "Erosion rates of cohesive soils." J. Hydr. Div., ASCE, 104(2), 279–283.
- Arulanandan, K. (1975). "Fundamental aspects of erosion in cohesive soils." J. Hydr. Div., ASCE, 101(5), 635–639.

- Arulanandan, K., Loganathan, P., and Krone, R. B. (1975). "Pore and eroding fluid influence on surface erosion of soil." *J. Geotech. Engrg. Div., ASCE*, 101(1), 51–66.
- ASTM D1587, American Society for Testing and Materials, Philadelphia, USA.
- Bhandari, G., Sarkar, S. S., and Rao, G. V. (1998). *Erosion control with geosynthetics, Geohorizon: State of art in geosynthetic technology*, A.A. Balkema, Rotterdam, Netherlands.
- Biedenharn, D. S., Elliott, C. M., and Watson, C. C. (1997). *The WES Stream Investigation and Streambank Stabilization Handbook*. US Army Engineer Waterways Experiment Station, Vicksburg, MS.
- Briaud J.-L., Ting F., Chen H.C., Cao Y., Han S.-W., Kwak K., "Erosion Function Apparatus for Scour Rate Predictions". *Journal of Geotechnical and Geoenvironmental Engineering*, ASCE, Vol.127, No. 2, 2001a, pp.105-113.
- Briaud J.-L., Ting F., Chen H.-C., Gudavalli R., Kwak K., Philogene B., Han S.-W., Perugu S., Wei G.S., Nurtjahyo P., Cao Y.W., Li Y., "SRICOS: Prediction of Scour Rate at Bridge Piers, TTI Report no. 2937-1 to the Texas DOT, 1999, Texas A&M University, College Station, Texas, USA.
- Briaud, J. L., Chen, H. C. Kwak K., Han S-W., Ting F., "Multiflood and Multilayer Method for Scour Rate Prediction at Bridge Piers", *Journal of Geotechnical and Geoenvironmental Engineering*, ASCE, Vol.127, No. 2, 2001b, pp.105-113.
- Briaud, J.-L., Ting, F., Chen, H.C., Gudavalli, S.R., Perugu, S., and Wei, G., "SRICOS: Prediction of Scour Rate in Cohesive Soils at Bridge Piers", *ASCE Journal of Geotechnical Engineering*, Vol.125, 1999, pp. 237-246.
- Cao Y., Wang J., Briaud J.L., Chen H.C., Li Y. Nurtjahyo P., 2002, "EFA Tests and the influence of Various Factors on the Erodibility of Cohesive Soils", *Proceedings of the First International Conference on Scour of Foundations*, Texas A&M University, Dpt. of Civil Engineering, College Station.
- Cao, Y., "The Influence of Certain Factors on the Erosion Functions of Cohesive Soil", *Master Thesis*, 2001, Texas A&M University, College Station, Texas, USA
- Chen, Y.H., Cotton, G.K., (1988), "Design of Roadside Channels with Flexible Linings," *Federal Highway Administration, Hydraulic Engineering Circular No. 15*.
- Choliaras, I.G., Tantos, V.A., Ntalos, G.A., Metaza, X.A., (2003), "The influence of soil conditions on the resistance of cohesive soils against erosion by overland flow," *Journal of International Research Publication*, Issue 3.
- Christensen, B. A. (1965). "Discussion of 'Erosion and deposition of cohesive soils,' by E. Partheniades." *J. Hydr. Div., ASCE*, 91(5), 301– 308.

- Coleman S.E., Andrews D.P., Webby M.G., (2002), "Overtopping Breaching of Non Cohesive Homogeneous Embankments", Journal of Hydraulic Engineering, Vol. 138, No. 9, ASCE, Reston, Virginia, USA.
- Coppin, N. J., and Richards, I. G. (1990). Use of Vegetation in Civil Engineering. Butterworths, London.
- Dodge, R.A., (1988), Overtopping Flow on Low Embankment Dams – Summary Report of Model Tests, REC-ERC-88-3, U.S. Bureau of Reclamation, Denver, Colorado.
- Dunn, I. S. (1959). "Tractive resistance to cohesive channels." J. Soil Mech. and Found. Div., ASCE, 85(3), 1–24.
- Einstein, H.A., El-Samni, E.S., 1949, "Hydrodynamic forces on a rough wall", Review of modern physics, 21, 520-524.
- Enger, P. F., Smerdon, E. T., and Masch, F. D. (1968). "Erosion of cohesive soils." J. Hydr. Div., ASCE, 94(4), 1017–1049.
- Fread, D.L., (1988), BREACH: An Erosion Model for Earthen Dam Failures, National Weather Service, National Oceanic and Atmospheric Administration, Silver Spring, Maryland.
- Gerritsen, H. (2006), "The 1953 Dike Failures in the Netherlands, Geo-Strata, March-April 2006, p18-21, Geo-Institute of the American Society of Civil Engineers, Reston, Virginia, USA.
- Gray, D. H. (1974). "Reinforcement and stabilization of soil by vegetation." J. Geotech. Engr. Div., ASCE, 100(GT6), 695-699.
- Gray, D. H., and Leiser, A. T. (1982). Biotechnical Slope Protection and Erosion Control. Van Nostrand Reinhold, New York.
- Gray, D. H., and Sotir, R. B. (1996). Biotechnical and Soil Bioengineering Slope Stabilization: a Practical Guide for Erosion Control. John Wiley & Sons, Inc., New York.
- Greenway, D. R. (1987). Vegetation and slope stability. In: M.G. Anderson, K.S. Richards (Eds.). Slope Stability: Geotechnical Engineering and Geomorphology, John Wiley & Sons, New York, pp. 187-230.
- Hanson, G.J., Cook, K.R., (2004), "Apparatus, test procedures, and analytical methods to measure soil erodibility in situ," Applied Engineering in Agriculture, American Society of Agricultural Engineers, Vol. 20, No. 4, pp. 455-462.
- Hanson, G.J., Cook, K.R., Hahn IV, W., (2001), "Evaluating headcut migration rates of earthen embankment breach tests," Written for Presentation at the 2001 ASAE Annual International Meeting, Paper No. 01-012080, Sacramento, California.

- Hanson, G.J., Cook, K.R., Hahn IV, W., Britton, S.L., (2003), "Evaluating erosion widening and headcut migration rates for embankment overtopping tests", Written for Presentation at the 2003 ASAE Annual International Meeting, Paper No. 032067, Las Vegas, Nevada.
- Hanson, G.J., Cook, K.R., Hahn IV, W., Britton, S.L., (2003), "Observed Erosion Processes During Embankment Overtopping Tests," Written for presentation at the 2003 ASAE Annual International Meeting, Paper No. 032066, Las Vegas, Nevada.
- Hanson, G.J., Cook, K.R., Hunt, S., (2005), "Physical modeling of overtopping erosion and breach formation of cohesive embankment," Transactions of the ASABE, Vol. 48, No. 5, pp. 1783-1794.
- Hanson, G.J., Simon, A., (2001), "Erodibility of cohesive streambeds in the loess area of the Midwestern USA", Hydrological Processes, Vol. 15, pp. 23–38.
- Hanson, G.J., Temple, D.M., Morris, M., Hassan, M., Cook, K., (2005), "Simplified Breach Analysis Model For Homogeneous Embankments: Part II, Parameter Inputs And Variable Scale Model Comparisons," Proceedings Of 2005 U.S. Society On Dams Annual Meeting And Conference, Salt Lake City, Utah, pp. 163-174.
- Hunt, S.L., Hanson, G.J., Cook, K.R., Kadavy, K.C., (2004), "Breach Widening Observations from Earthen Embankment Tests," American Society of Agricultural Engineers/Canadian Society for Engineering Annual International Meeting, Ottawa, Canada, Paper No. 042080.
- Johnston A. (2003), "Range of Allowable Shear Stresses by Depth and Slope", personal communication.
- Kelly, E. K., and Gularte, R. C. (1981). "Erosion resistance of cohesive soils." J. Hydr. Div., ASCE, 107(10), 1211–1224.
- Li, M.-H., and Eddleman, K. E. (2002). "Biotechnical engineering as an alternative to traditional engineering methods: a biotechnical streambank stabilization design approach." Landscape and Urban Planning 60(4), 225-242.
- Lyle, W. M., and Smerdon, E. T. (1965). "Relation of compaction and other soil properties to erosion and resistance of soils." Trans., ASAE, American Society of Agricultural Engineers, St. Joseph, Mich., 8(3).
- Mitchell, J.K., 1993, "Fundamentals of Soil Behavior", 2nd Ed., John Wiley and Sons, New York.
- Moody L.F., "Friction Factors for Pipe Flow", Transaction of the American Society of Civil Engineers, 1944, Vol. 66, Reston, Virginia, USA.
- Munson, B. R., Young, D. F., and Okiishi, T. H. (1990). Fundamentals of fluid mechanics. Wiley, New York.

- Nairn, R.B., (1986), "Physical Modeling of Wave Erosion on Cohesive Profiles," Proceedings, Symposium on Cohesive Shores, Burlington, Ontario.
- Ralston, D.C., (1987), "Mechanics of embankment erosion during overflow," Proceedings of the 1987 National Conference on Hydraulic Engineering, Hydraulics Division of ASCE, pp. 733-738.
- Richardson, E. V., and Davis, S. R. (1995). "Evaluating scour at bridges." Rep. No. FHWA-IP-90-017 (HEC 18), Federal Highway Administration, Washington, D.C.
- Shaikh, A., Ruff, J. F., and Abt, S. R. (1988). "Erosion rate of compacted Na-montmorillonite soils." J. Geotech. Engrg., ASCE, 114(3), 296– 305.
- Shields, A. (1936). "Anwendung der Aehnlichkeits-Mechanik und der Turbulenzforschung auf die Geschiebebewegung." Preussische Versuchsanstalt für Wasserbau and Schiffbau, Berlin (in German).
- Shields, A., "Application of similarity principles, and turbulence research to bed-load movement," 1936, California Institute of Technology, Pasadena (translated from German).
- Smerdon, E. T., and Beasley, R. P. (1959). "Tractive force theory applied to stability of open channels in cohesive soils." Res. Bull. No. 715, Agricultural Experiment Station, University of Missouri, Columbia.
- Styczen, M. E., and Morgan, R. P. C. (1995). Engineering properties of vegetation. In: R.P.C. Morgan, R.J. Rickson (Eds.). Slope Stabilization and Erosion Control: A Bioengineering Approach. E & FN Spon, London, pp. 5-58.
- Temple, D.M., Hanson, G.J., Neilsen, M.L., Cook, K.R., (2005), "Simplified Breach Analysis Model For Homogeneous Embankments: Part I, Background And Model Components," Proceedings Of The 2005 U.S. Society On Dams Annual Meeting And Conference, Salt Lake City, Utah, pp. 151-161.
- USACE (1999). Guidelines for Landscape Planting and Vegetation Management at Floodways, Levees, and Embankment Dams. Engineering Manual 1110-2-301, U.S. Army Corps of Engineers, Washington, D.C.
- USACE, (2000), "Engineering and Design – Design and Construction of Levees," Publication No. EM 1110-2-1913.
- Vanoni, V. A., "Sedimentation Engineering", ASCE-Manuals and Reports on Engineering Practice no. 54, 1975, prepared by the ASCE task committee.
- White, C.M., 1940, "The Equilibrium of grains on the bed of a stream", Proc. Royal Soc. of London, 174(958), 322-338.
- Wu, T.H. (1995). Slope stabilization. In: R.P.C. Morgan, R.J. Rickson (Eds.). Slope Stabilization and Erosion Control: A Bioengineering Approach. E & FN Spon, London, pp. 221-264.

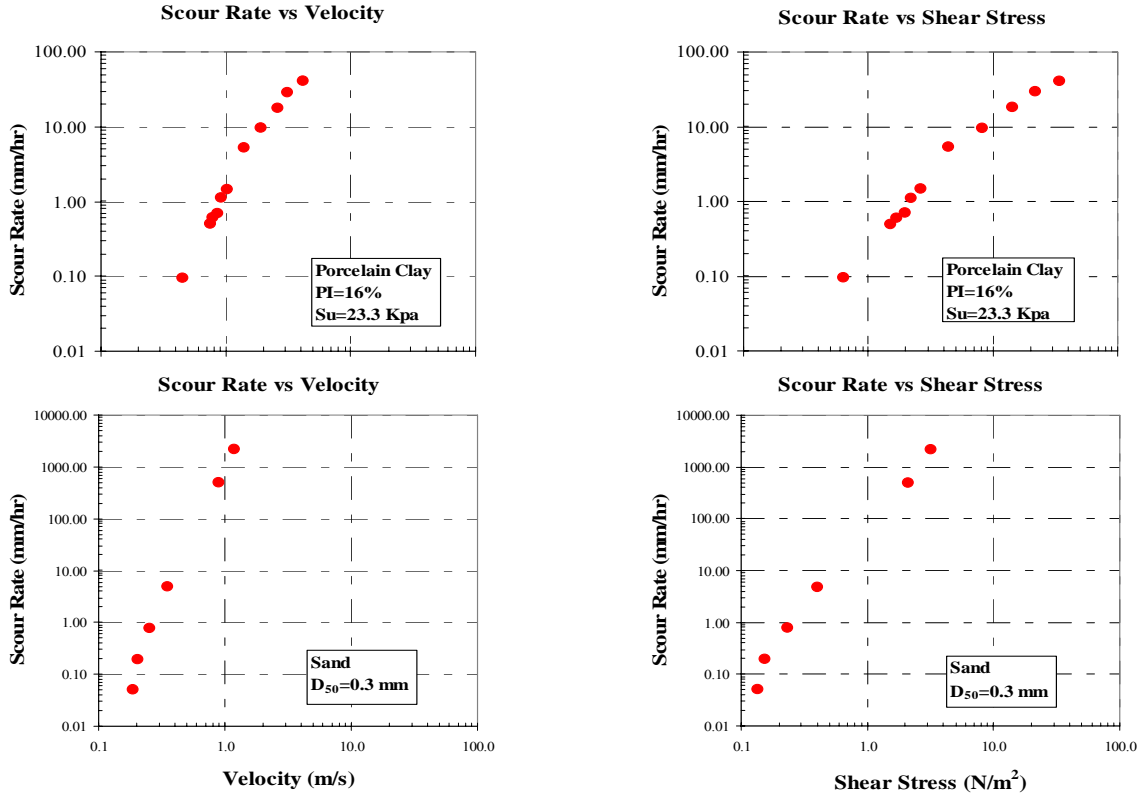


Figure 9.1: Erodibility function for a clay and for a sand.

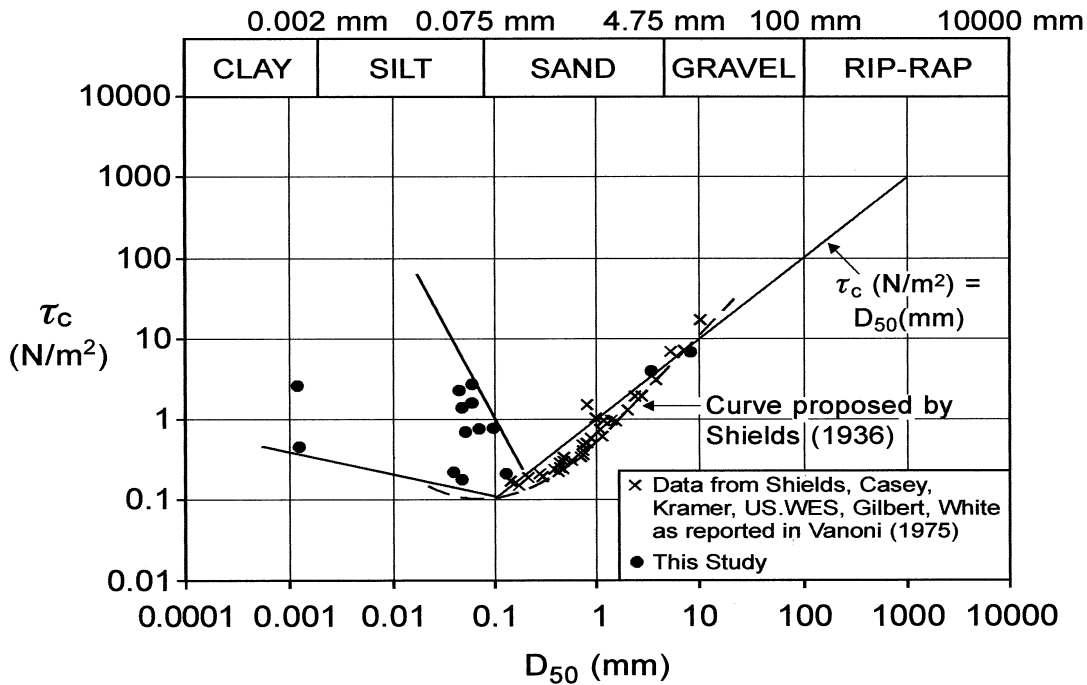


Figure 9.2: Critical shear stress versus mean soil grain size.

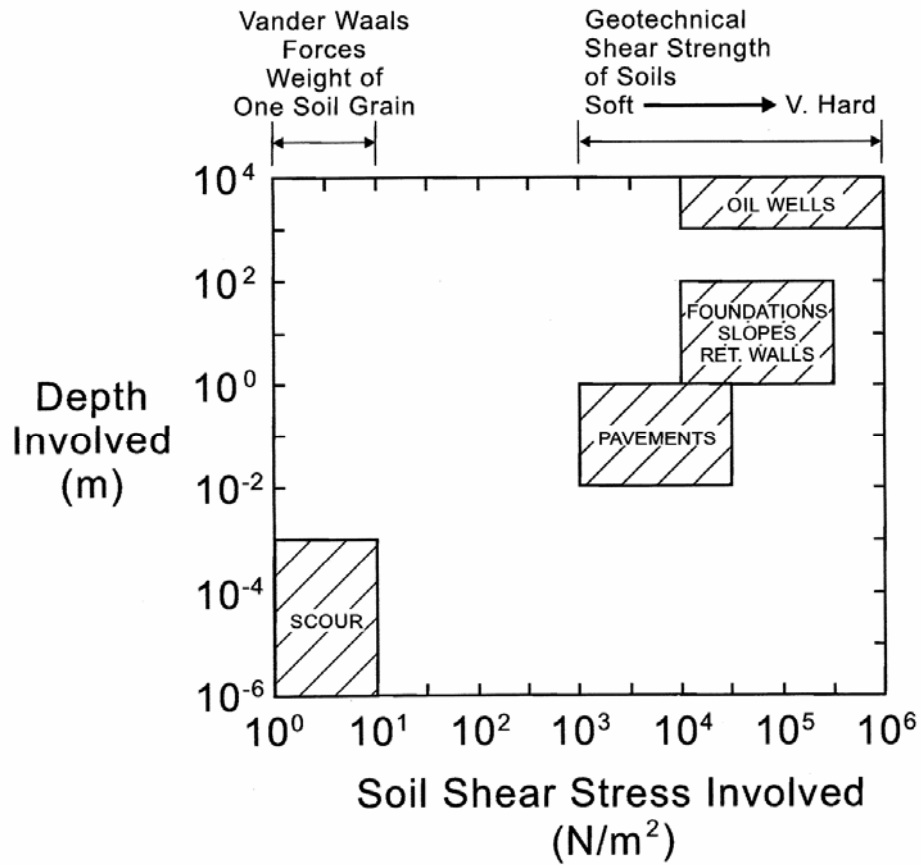


Figure 9.3: Magnitude of shear stresses involved in various fields of engineering.

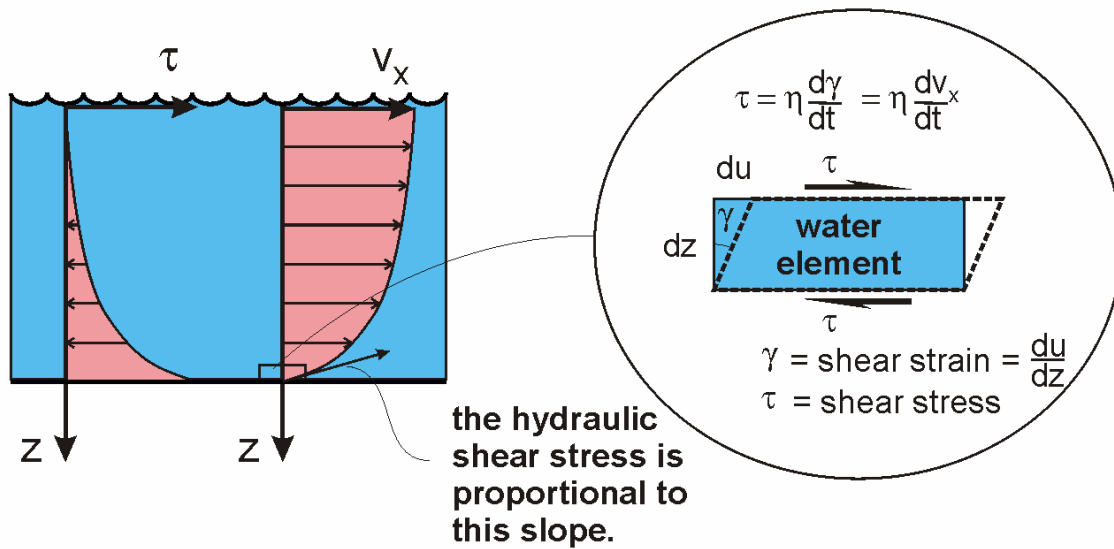


Figure 9.4: Velocity and shear stress within the flow depth.

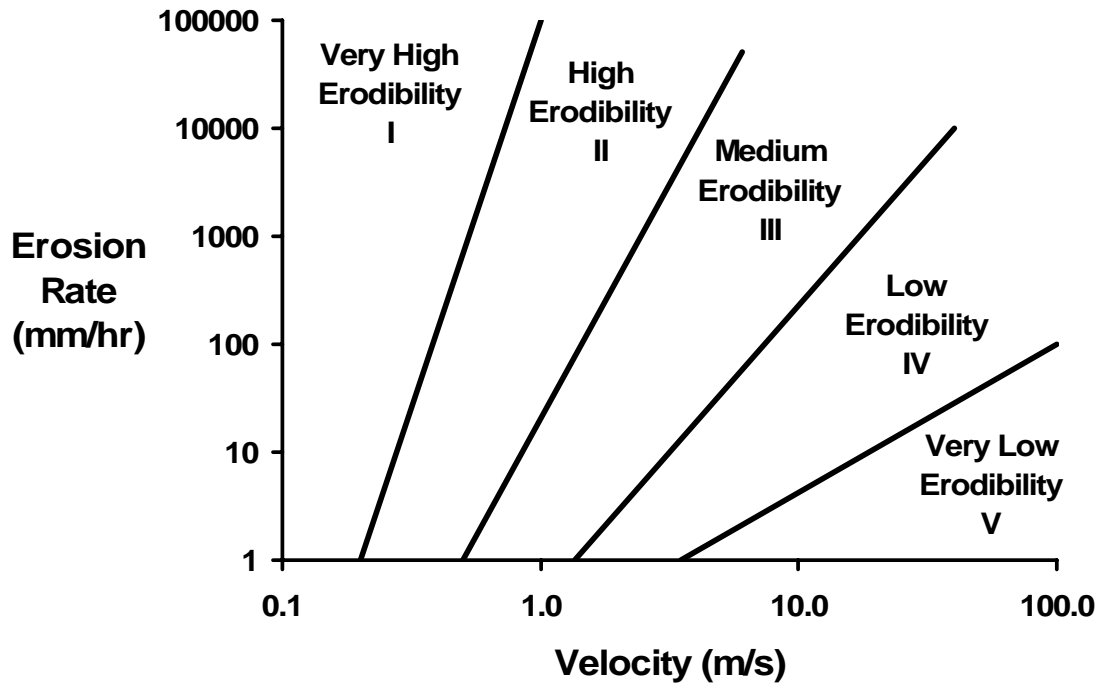


Figure 9.5: Erosion Categories.

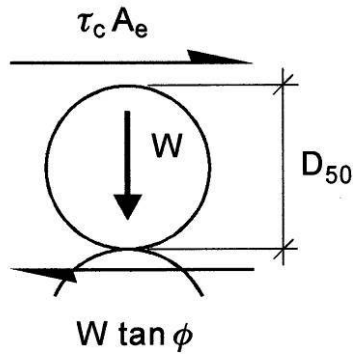


Figure 9.6: Particle diagram for a simple sliding mechanism.

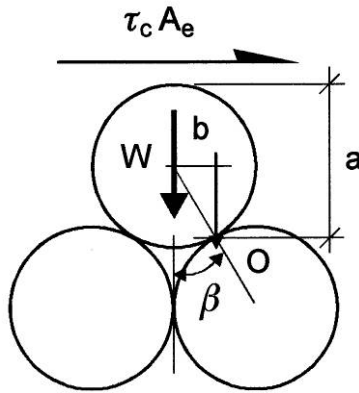


Figure 9.7: Particle diagram for a simple rolling mechanism.

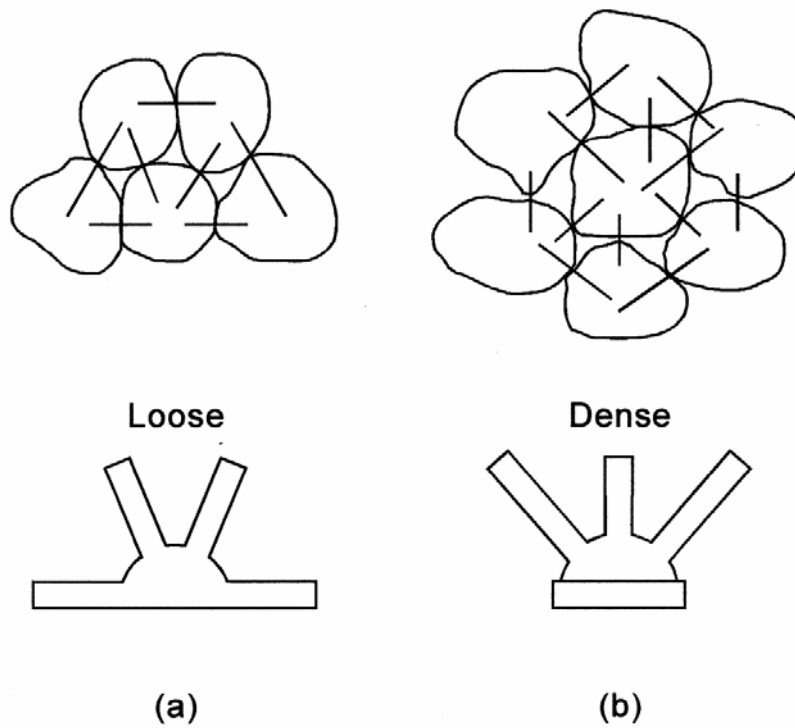


Figure 9.8: Contact angle distributions in coarse grained soils.

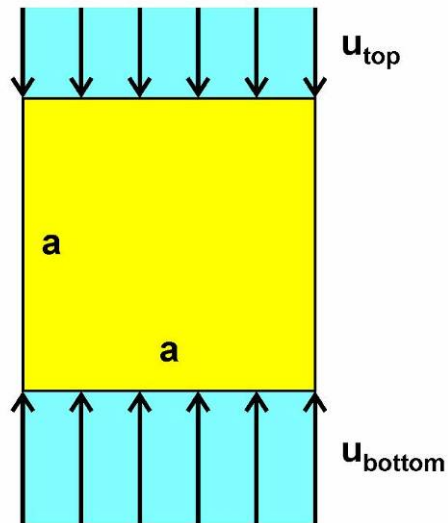


Figure 9.9: Particle diagram for a simple plucking mechanism.

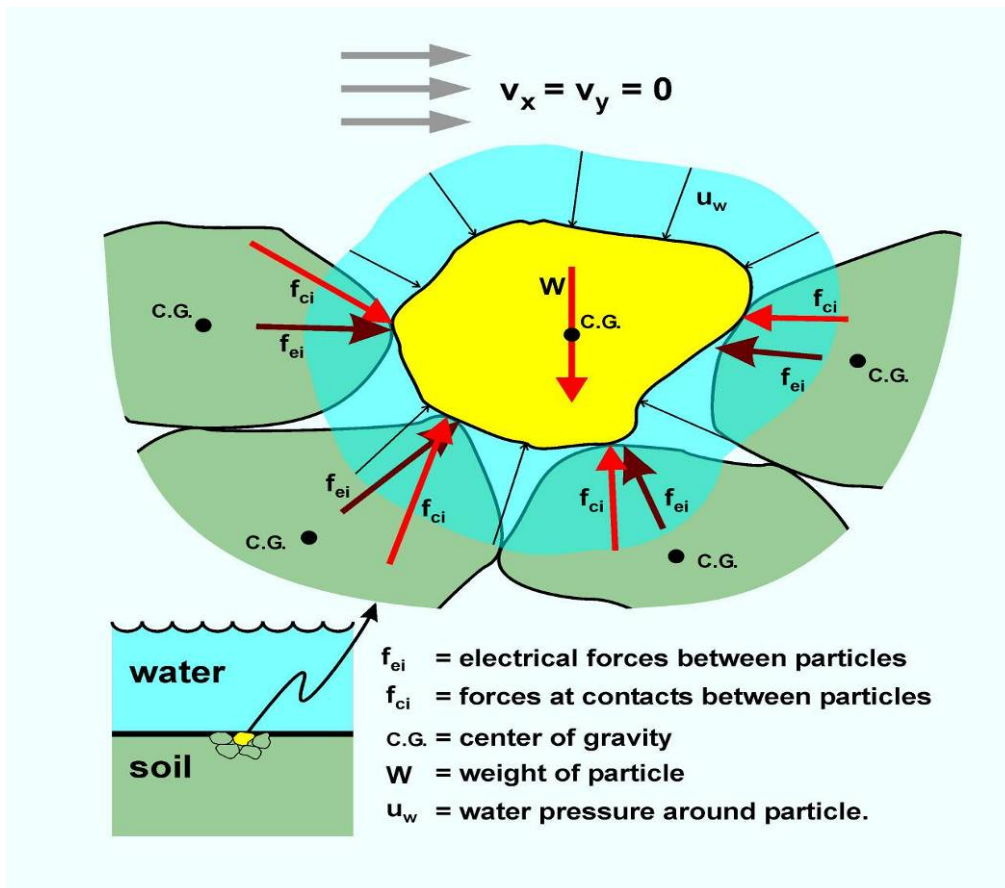


Figure 9.10: Forces and pressure on particle: no flow condition

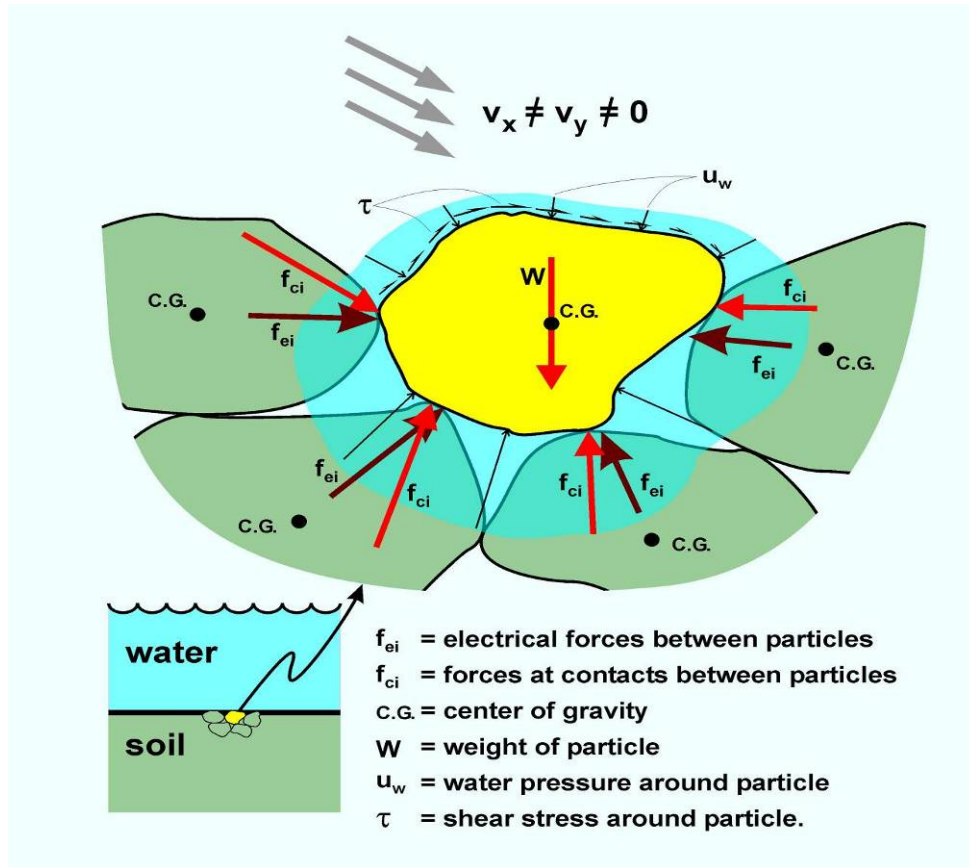


Figure 9.11: Forces and pressure on particle: flow condition.

Table 9.1: Gravity and Van der Waals Forces for Sand and Clay Particles

| | Sand particle | Clay particle |
|--|------------------------|------------------------|
| Diameter d (m) | 2×10^{-3} | 1×10^{-6} |
| Weight W (N) | 1.1×10^{-3} | 1.36×10^{-13} |
| Van der Waals attraction F_{VDW} (N) | 7.85×10^{-23} | 3.14×10^{-16} |
| F_{VDW}/W | 7.1×10^{-20} | 2.3×10^{-3} |

Table 9.2: Measured Critical Shear Stress in Clays

| Authors | Range of τ_c (N/m ²) |
|--|---------------------------------------|
| Dunn (1959) | 2–25 |
| Enger et al. (1968) | 15–100 |
| Hydrotechnical Construction, Moscow (1936) | 1–20 |
| Lyle and Smerdon (1965) | 0.35–2.25 |
| Smerdon and Beasley (1959) | 0.75–5 |
| Arulanandan et al. (1975) | 0.1–4 |
| Arulanandan (1975) | 0.2–2.7 |
| Kelly and Gularte (1981) | 0.02–0.4 |

Table 9.3: Measured Erosion Rates in Clay

| Authors | Results | Inferred scour rate (mm/hr)* |
|--------------------------------|-------------------------------------|------------------------------|
| Richardson, Davis (1995) | Maximum scour depth reached in days | 10-100 |
| Arulanandan et al. (1975) | 1-4 g/cm ² /min | 300-1200 |
| Shaikh et al. (1988) | 0.3-0.8 N/m ² /min | 9-24 |
| Ariathurai, Arulanandan (1978) | 0.005-0.09 g/cm ² /min | 1.5-27 |
| Kelly, Gularte (1981) | 0.0057-0.01 g/cm ² /s | 100-180 |

* Erosion rate $dz/dt = (\text{weight loss rate per unit area } dw/a \text{ dt})/(\text{unit weight } \gamma)$

Table 9.4: Factors Influencing the Erodibility of Fine Grained Soils

| <u>When this parameter increases</u> | <u>Erodibility</u> |
|--------------------------------------|--------------------|
| Soil water content | |
| Soil unit weight | decreases |
| Soil plasticity Index | decreases |
| Soil undrained shear strength | increases |
| Soil void ratio | increases |
| Soil swell | increases |
| Soil mean grain size | |
| Soil percent passing sieve #200 | decreases |
| Soil clay minerals | |
| Soil dispersion ratio | increases |
| Soil cation exchange capacity | |
| Soil sodium absorption ratio | increases |
| Soil pH | |
| Soil temperature | increases |
| Water temperature | increases |
| Water chemical composition | |

Table 9.5: Database of EFA tests

| | |
|--|-----------------|
| Woodrow Wilson Bridge (Washington) | Tests 1 to 12 |
| South Carolina Bridge | Tests 13 to 16 |
| National Geotechnical Experimentation Site (Texas) | Tests 17 to 26 |
| Arizona Bridge (NTSB) | Test 27 |
| Indonesia samples | Tests 28 to 33 |
| Porcelain clay (man-made) | Tests 34 to 72 |
| Bedias Creek Bridge (Texas) | Tests 73 to 77 |
| Sims Bayou (Texas) | Tests 78 to 80 |
| Brazos River Bridge (Texas) | Test 81 |
| Navasota River Bridge (Texas) | Tests 82 and 83 |
| San Marcos River Bridge (Texas) | Tests 84 to 86 |
| San Jacinto River Bridge (Texas) | Tests 87 to 89 |
| Trinity River Bridge (Texas) | Tests 90 and 91 |

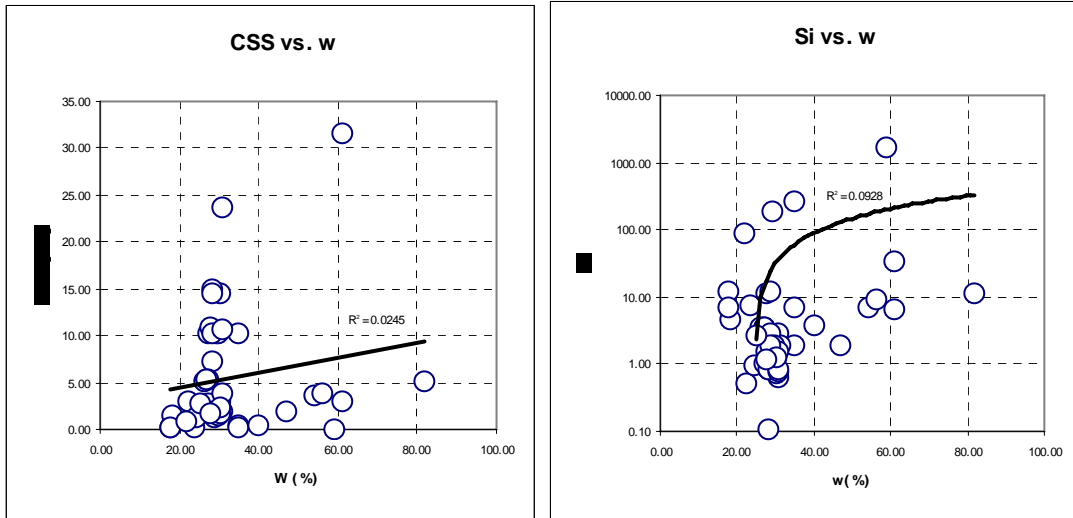


Figure 9.12: Erosion properties as a function of water content.

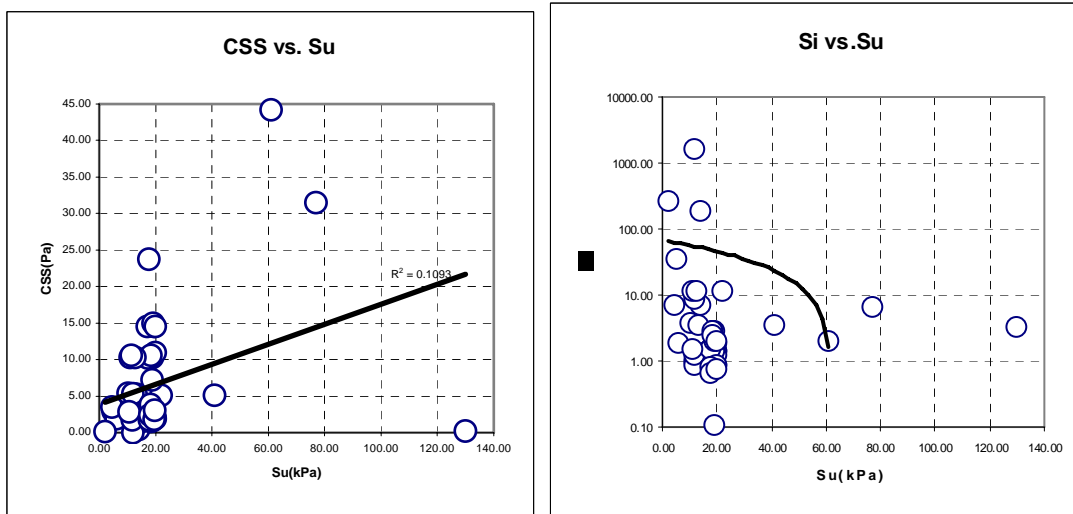


Figure 9.13: Erosion properties as a function of undrained shear strength.

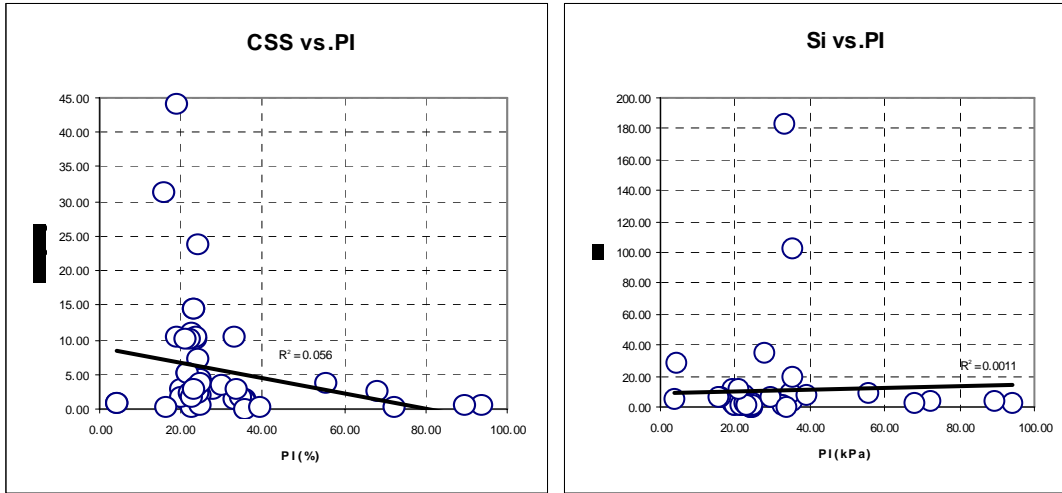


Figure 9.14: Erosion properties as a function of plasticity index.

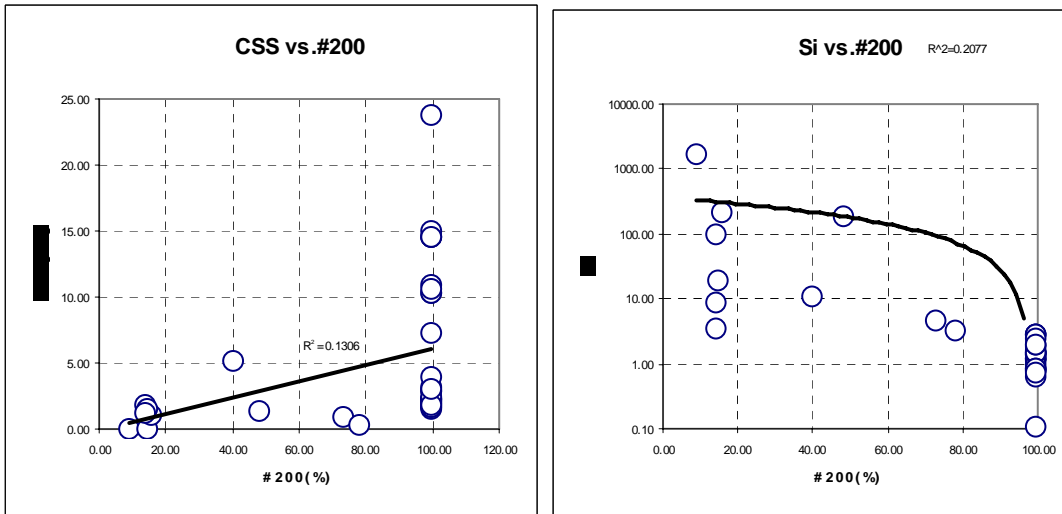
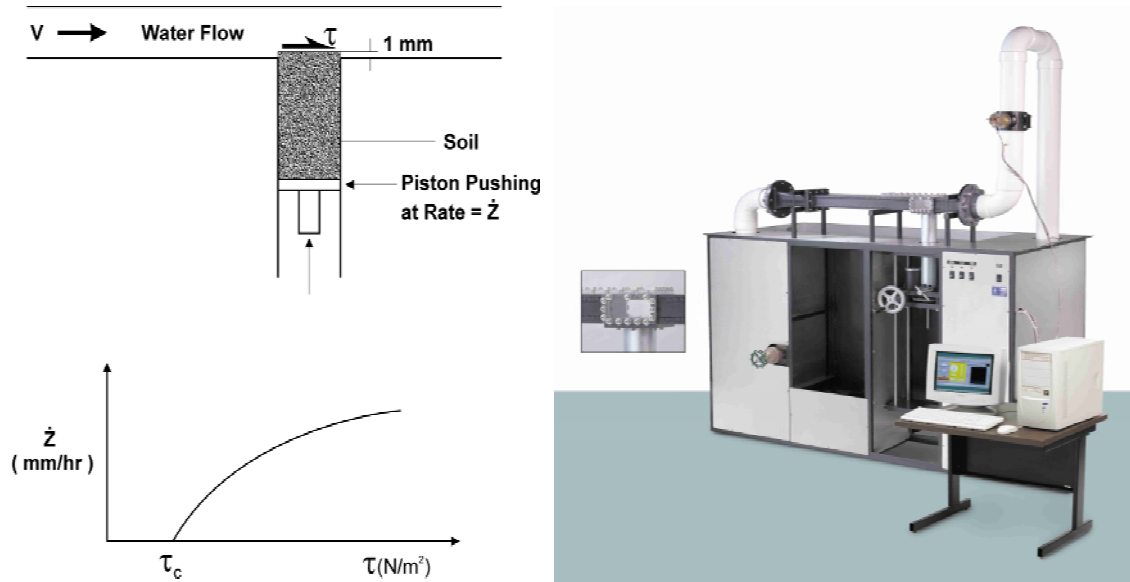
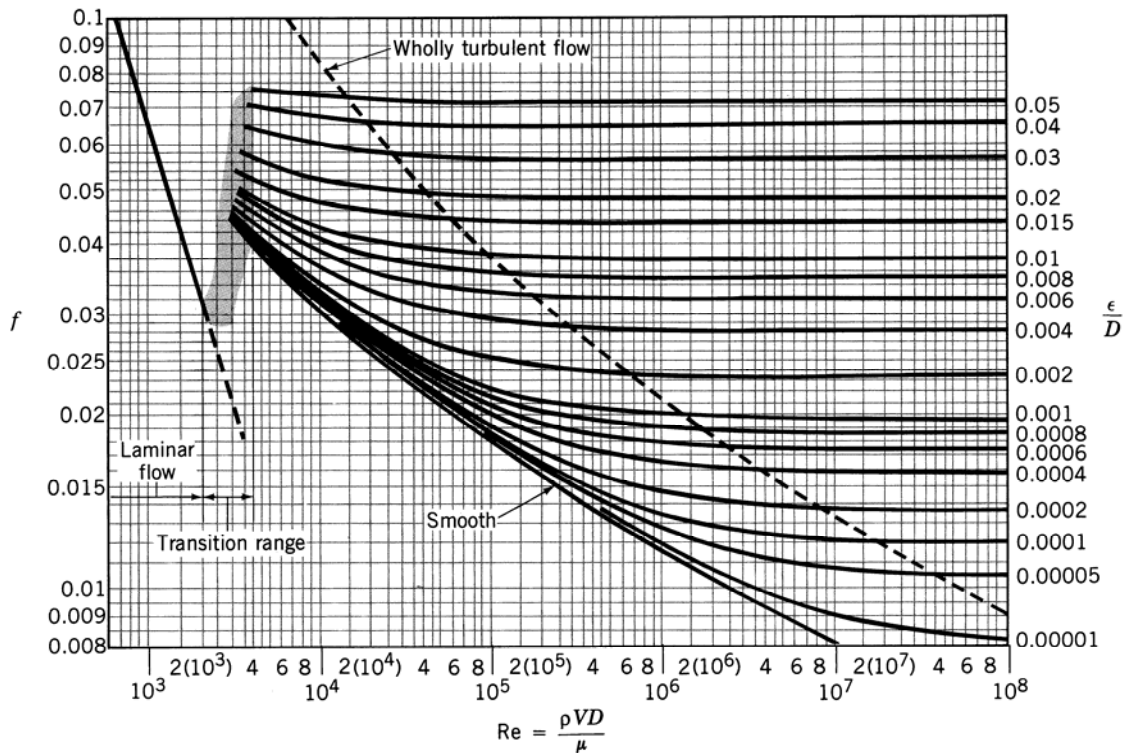


Figure 9.15: Erosion properties as a function of percent passing sieve #200.



Source: Briaud et al (2001)

Figure 9.16: EFA (Erosion Function Apparatus).



Source: Munson et al (1990)

Figure 9.17: Moody Chart.

Table 9.6: Procedures for Levee Design and Construction (USACE, 2000)

| Major and Minimum Requirements | |
|--------------------------------|--|
| Step | Procedure |
| 1 | Conduct geological study based on a thorough review of available data including analysis of aerial photographs. Initiate preliminary subsurface explorations. |
| 2 | Analyze preliminary exploration data and from this analysis establish preliminary soil profiles, borrow locations, and embankment sections. |
| 3 | Initiate final exploration to provide: <ul style="list-style-type: none"> a. Additional information on soil profiles. b. Undisturbed strengths of foundation materials. c. More detailed information on borrow areas and other required excavations. |
| 4 | Using the information obtained in Step 3: <ul style="list-style-type: none"> a. Determine both embankment and foundation soil parameters and refine preliminary sections where needed, noting all possible problem areas. b. Compute rough quantities of suitable material and refine borrow area locations. |
| 5 | Divide the entire levee into reaches of similar foundation conditions, embankment height, and fill material and assign a typical trial section to each reach. |
| 6 | Analyze each trial section as needed for: <ul style="list-style-type: none"> a. Underseepage and through seepage. b. Slope stability. c. Settlement. d. Trafficability of the levee surface. |
| 7 | Design special treatment to preclude any problems as determined from Step 6. Determine surfacing requirements for the levee based on its expected future use. |
| 8 | Based on the results of Step 7, establish final sections for each reach. |
| 9 | Compute final quantities needed; determine final borrow area locations. |
| 10 | Design embankment slope protection. |

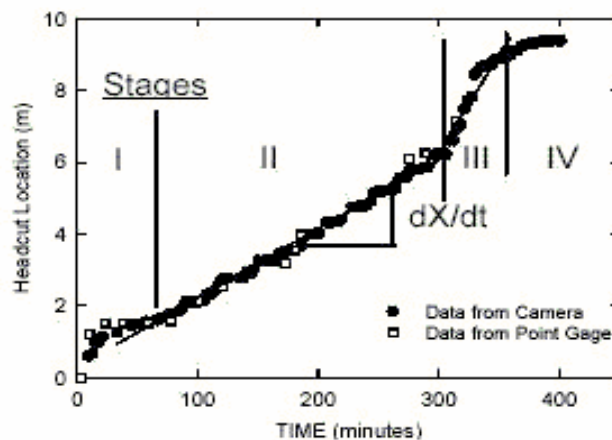
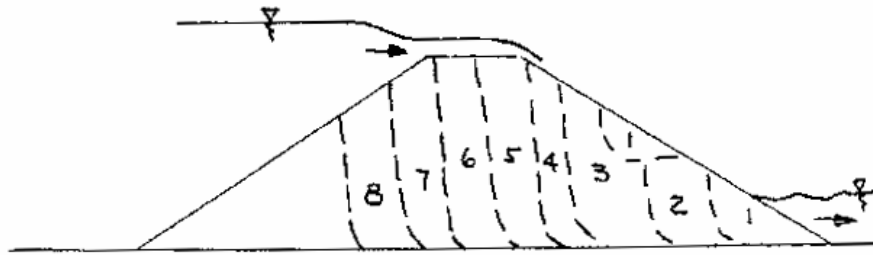
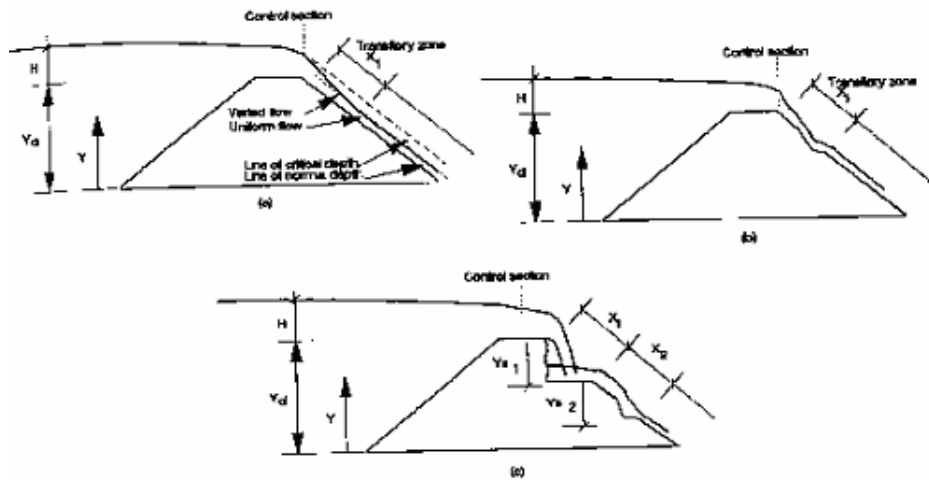


Figure 9.18: Headcut Location as a Function of Time.



Source: Ralston (1987)

Figure 9.19: Stages of Progressive Erosion.



Source: AlQaser, Ruff (1993)

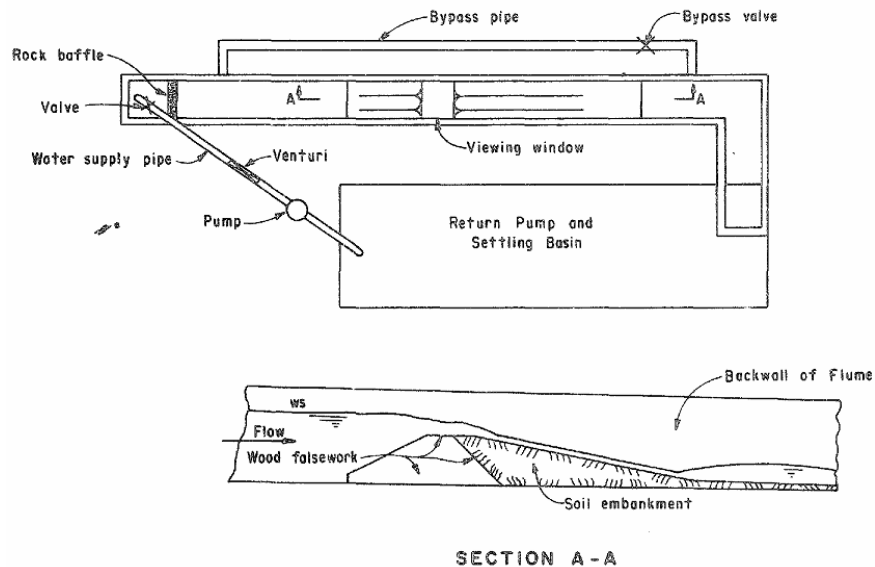
Figure 9.20: Progressive Failure of an Overtopped Embankment.

Table 9.7: Summary of Dam Break Computer Models (AlQaser, 1991)

| Model (Yr of Publ) | Hydrodynamic Approach | Sediment Transport | Solution Algorithm | Breach Morphology | Characteristic Parameters | Other Features | | |
|--|---|---|---|---|---|--|--|--|
| Cristofano (1965) | Broad-crested weir hydraulic relation | Empirical relation | Manual- iterative | Constant width | Proportionality constant, angle of repose | No tailwater effects, no sloughing | | |
| Harris & Wagner (1967) | | Schoklitsch bed- load formula | Numerical | Parabolic shape | Grain size, critical discharge value, breach dimensions and slope | No tailwater effects, no sloughing | | |
| BRDAM Brown & Rogers (1977, 1981) | | Linear pre- determined rate of erosion | | Rectangular, triangular, trapezoidal | Failure duration tim, terminal size and shape of breach | | | |
| DAMBRK – Fread (1977) | St. Venant system of equations | Empirical relation | Preissmann’s 4- point finite difference | Regime type relation between top width and flow rate | Coefficients of the regime relation, critical shear stress | No sloughing | | |
| Lou (1981) | | Meyer-Peter and Mueller bed-load formula | | | | | | |
| BREACH – Fread (1984) | Broad-crested weir hydraulic relation | Einstein-Brown bed-load formula | Numerical iterative | Rectangular or trapezoidal | Friction angle, dimensionless shear stress $1/\psi$ | Tailwater effects and sloughing are included | | |
| BEED – Singh 1989) | | linear predetermined rate of erosion | | | | | Dam height above the breach volume of water in the reservoir | Neglects the triggering mechanism of failure, sloughing is incorporated |
| Froelich (1990) | | Regression relations to predict breach parameters and time of failure | | | | | | |

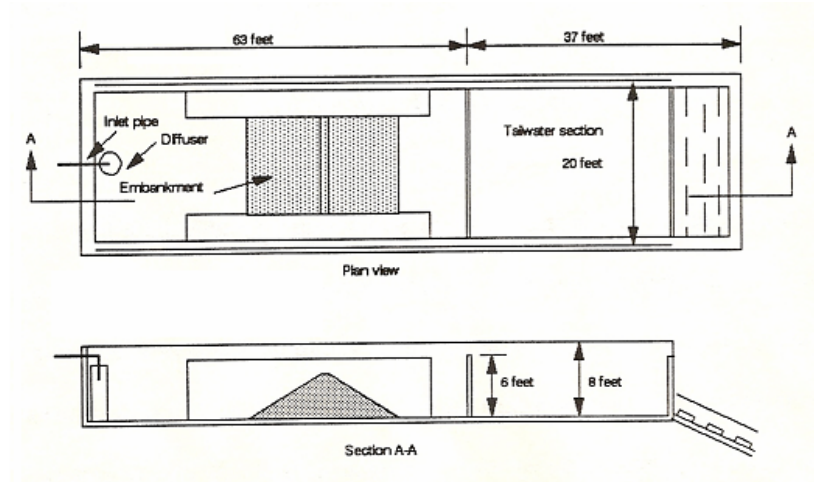
Table 9.8: Results from Flume Tests (Nairn, 1986)

| Run | Description | Duration | Erosion Rate ($m^3/m\ hr$) |
|-----|---|----------------------|---|
| A | no bluff, composite slope, sand veneer | 6 hrs. | 0.0066 |
| B | bluff, composite slope, toe submerged 3 cm, sand veneer | 6 hrs. | 0.0046 |
| C | bluff, composite slope, toe submerged 5 cm, no sand | 6 hrs. | 0.0127 |
| F | bluff, constant 1:20 slope, toe at NWL, no veneer | 3.5 hrs. 6.5 hrs. | 0.0109 0.0098 |
| G | bluff, constant 1:20 slope, toe at NWL, sand veneer | 1 hr. | negligible, profile armoured with sand |



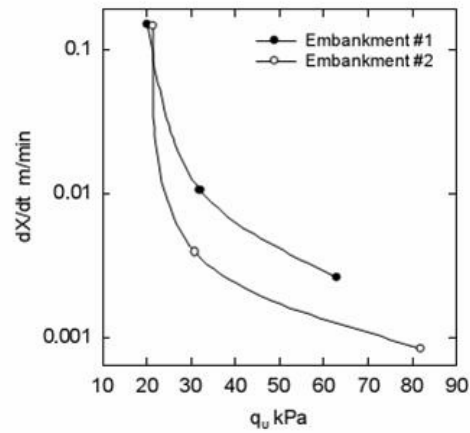
Source: Dodge (1988)

Figure 9.21: Laboratory Test Facility.



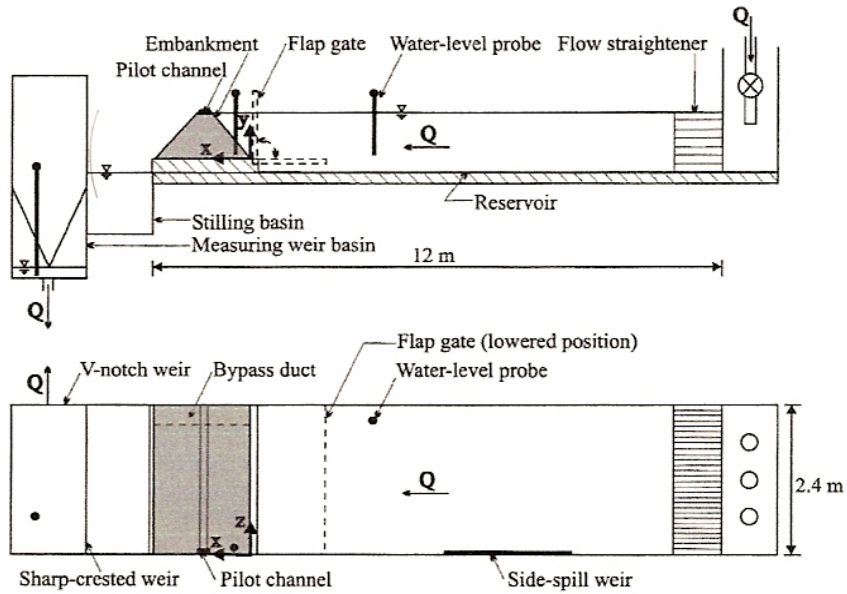
Source: AlQaser (1991)

Figure 9.22: Testing Facility.



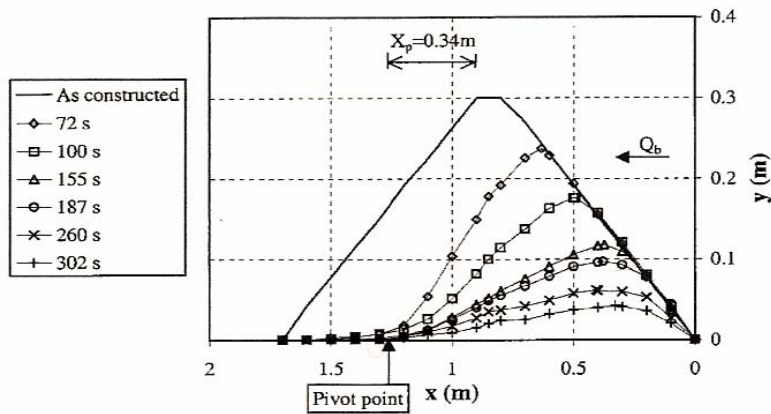
Source: Hanson et al. (2001)

Figure 9.23: Migration Rate vs. Unconfined Compression Tests.



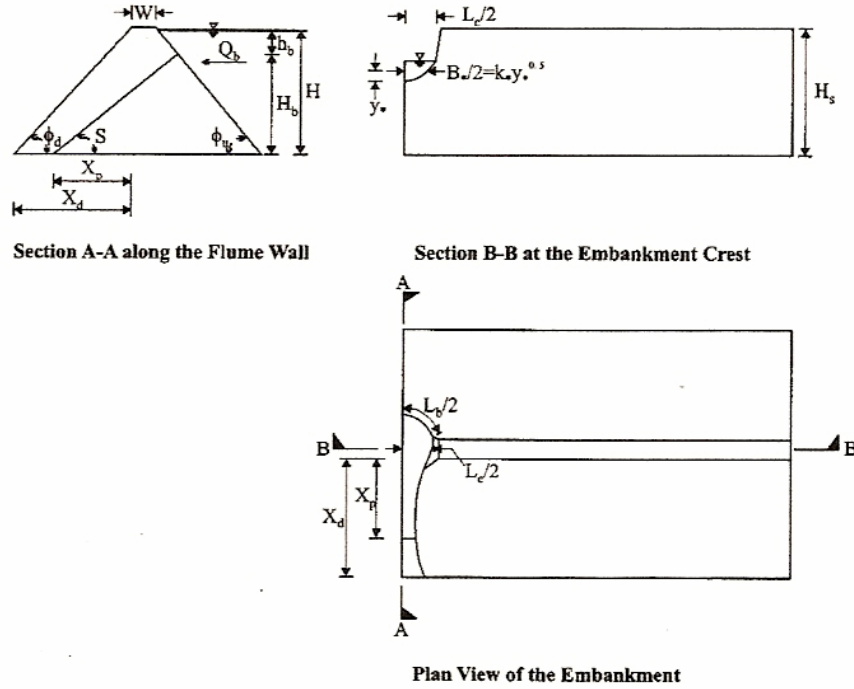
Source: Coleman et al. (2002)

Figure 9.24 : Experimental Setup.



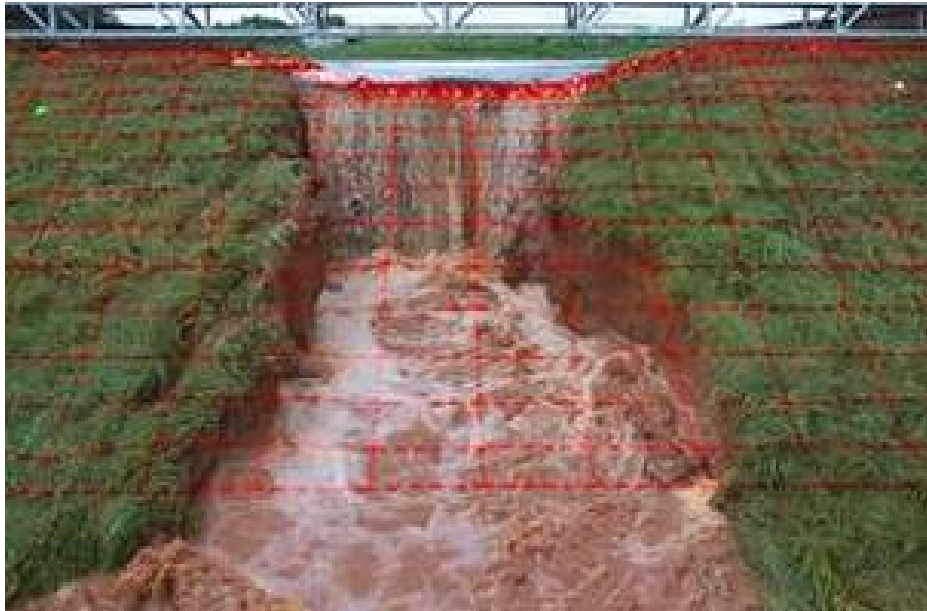
Source: Coleman et al. (2002)

Figure 9.25: Longitudinal Profiles Along Breach Channel Centerline for Medium-Sand Embankment.



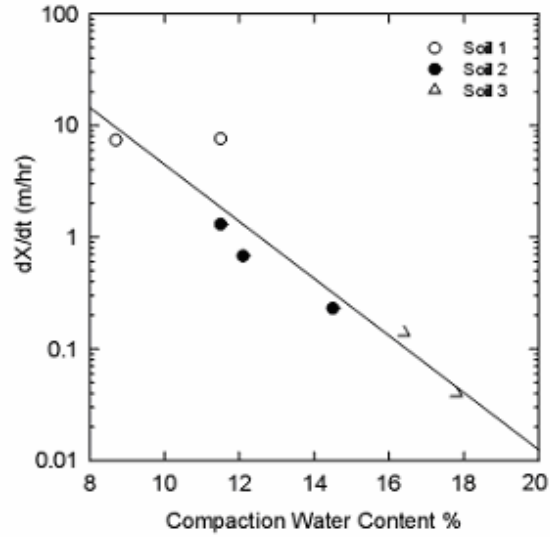
Source: Coleman et al. (2002)

Figure 9.26: Geometry Parameters for Breached Embankment.



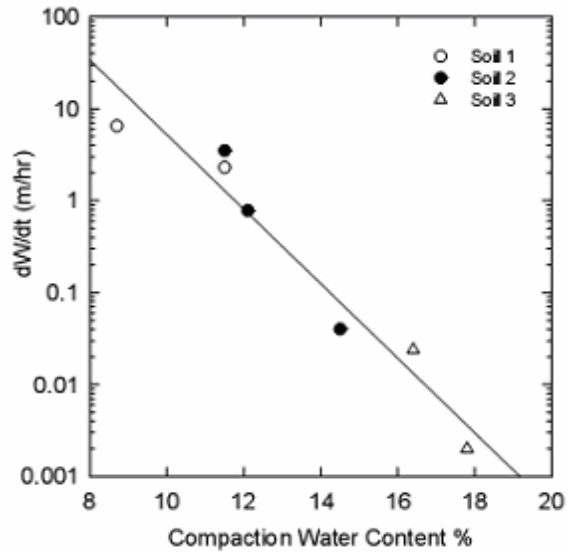
Source: Hanson et al. (2003)

Figure 9.27: Photographic Measurements of Erosion Width.



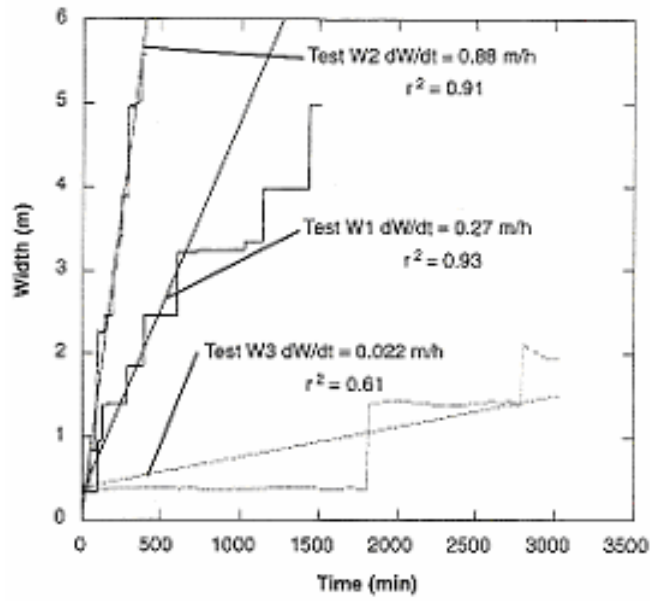
Source: Hanson et al. (2003)

Figure 9.28: Headcut Migration Rate vs. Compaction Water Content.



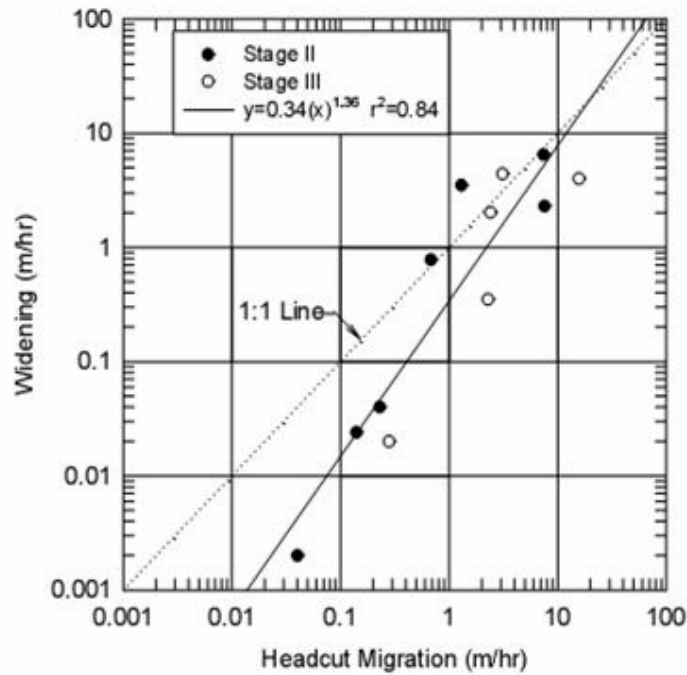
Source: Hanson et al. (2003)

Figure 9.29: Rate of Erosion Widening vs. Compaction Water Content.



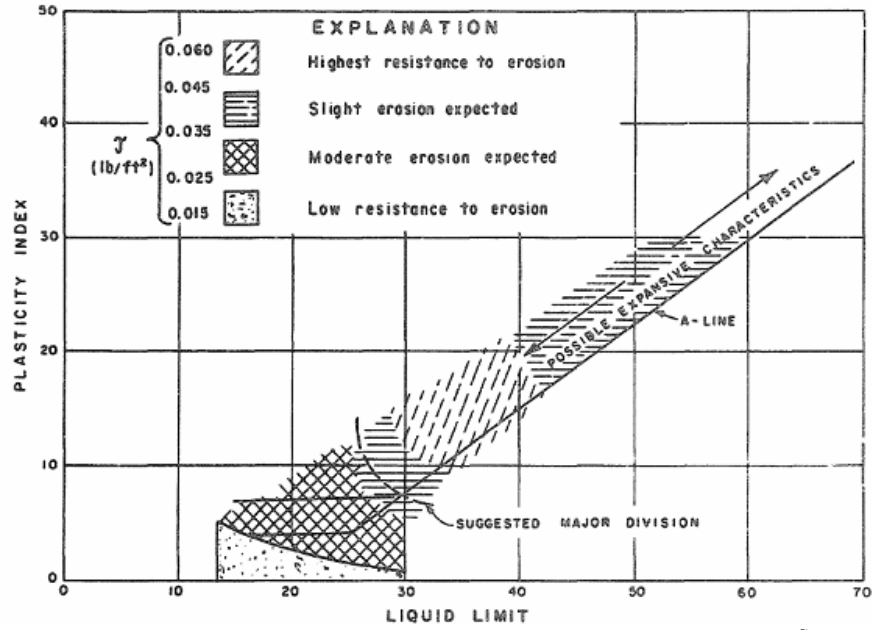
Source: Hunt et al. (2004)

Figure 9.30: Breach Width vs. Time.



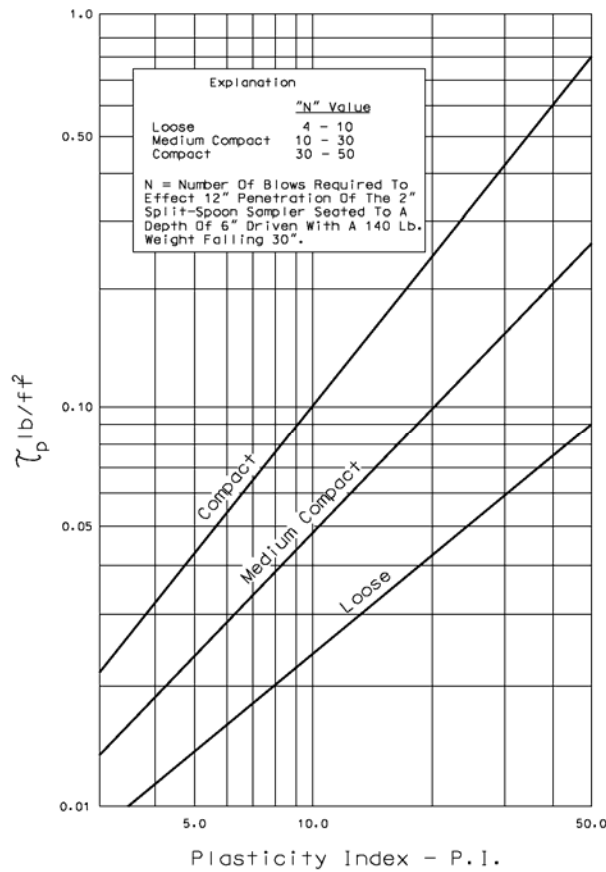
Source: Hanson et al., (2003)

Figure 9.31: Headcut Migration Rate vs. Rate of Widening.



Source: Dodge (1988)

Figure 9.32: Erosion Characteristics with respect to Plasticity.



Source: Chen & Cotton (1998)

Figure 9.33: Permissible Shear Stress for Cohesive Soils.



Figure 9.34: Difference in erosion resistance between grass cover and no grass cover.

RANGES OF SHEAR (pounds per square foot) BY DEPTH AND SLOPE

Note: This is Example A of a chart for a region with 30-40 inches of rainfall a year (good veg.) Generally "good soil" for vegetation growth. Soil silt, sand, clay mixture. The user should further refine this Example to a specific area of use.

Note: This assumes a "hydraulically wide" channel with generally straight alignment shear (psf) = unit wt of water (pcf) * depth (ft) * slope (ft/ft). If the channel is "hydraulically narrow" then replace D with R (area / wp)

Shear around bends can be greater than these values depending upon ratio of bend radius to bottom width. This chart is intended to be used as a quick visual guide and does not take the place of individual site analysis. The divisions between the different levels are "fuzzy" and should not be taken literally off of this chart.

Legend: Tan = soil can handle under 0.5 psf (depending upon type of soil)
 Green = grasses under 3 or 4 psf (depending upon type and condition of vegetation)
 Yellow = soft armor, geosynthetic matting, under 6 to 8 psf
 Red = hard armor, over 7 to 8 psf

Note: The colored "ranges" change from Example A to B to C

| D (ft) | 0.001 | 0.002 | 0.003 | 0.004 | 0.005 | 0.006 | 0.007 | 0.008 | 0.009 | 0.010 | 0.012 | 0.014 | 0.016 | 0.018 | 0.020 | 0.025 | 0.030 | 0.035 | 0.040 | 0.045 | 0.050 | 0.055 | 0.060 |
|--------|-------|-------|-------|-------|-------|-------|-------|-------|-------|-------|-------|-------|-------|-------|-------|-------|-------|-------|-------|-------|-------|-------|-------|
| 0.1 | 0.01 | 0.01 | 0.02 | 0.03 | 0.04 | 0.04 | 0.05 | 0.06 | 0.06 | 0.07 | 0.07 | 0.09 | 0.10 | 0.11 | 0.12 | 0.16 | 0.19 | 0.22 | 0.25 | 0.28 | 0.31 | 0.34 | 0.37 |
| 0.3 | 0.02 | 0.04 | 0.06 | 0.07 | 0.09 | 0.11 | 0.13 | 0.15 | 0.17 | 0.19 | 0.22 | 0.26 | 0.30 | 0.34 | 0.37 | 0.47 | 0.56 | 0.66 | 0.75 | 0.84 | 0.94 | 1.03 | 1.12 |
| 0.5 | 0.03 | 0.06 | 0.09 | 0.12 | 0.16 | 0.19 | 0.22 | 0.25 | 0.28 | 0.31 | 0.37 | 0.44 | 0.50 | 0.56 | 0.62 | 0.78 | 0.94 | 1.09 | 1.25 | 1.40 | 1.56 | 1.72 | 1.87 |
| 0.7 | 0.04 | 0.09 | 0.13 | 0.17 | 0.22 | 0.26 | 0.31 | 0.35 | 0.39 | 0.44 | 0.52 | 0.61 | 0.70 | 0.79 | 0.87 | 1.09 | 1.31 | 1.53 | 1.75 | 1.97 | 2.18 | 2.40 | 2.62 |
| 1.0 | 0.06 | 0.12 | 0.19 | 0.25 | 0.31 | 0.37 | 0.44 | 0.50 | 0.56 | 0.62 | 0.75 | 0.87 | 1.00 | 1.12 | 1.25 | 1.56 | 1.87 | 2.18 | 2.50 | 2.81 | 3.12 | 3.43 | 3.74 |
| 1.2 | 0.07 | 0.15 | 0.22 | 0.30 | 0.37 | 0.45 | 0.52 | 0.60 | 0.67 | 0.75 | 0.90 | 1.05 | 1.20 | 1.35 | 1.50 | 1.87 | 2.25 | 2.62 | 3.00 | 3.37 | 3.74 | 4.12 | 4.49 |
| 1.4 | 0.09 | 0.17 | 0.26 | 0.35 | 0.44 | 0.52 | 0.61 | 0.70 | 0.79 | 0.87 | 1.05 | 1.22 | 1.40 | 1.57 | 1.75 | 2.18 | 2.62 | 3.06 | 3.49 | 3.93 | 4.37 | 4.80 | 5.24 |
| 1.6 | 0.10 | 0.20 | 0.30 | 0.40 | 0.50 | 0.60 | 0.70 | 0.80 | 0.90 | 1.00 | 1.20 | 1.40 | 1.60 | 1.80 | 2.00 | 2.50 | 3.00 | 3.49 | 3.99 | 4.49 | 4.99 | 5.49 | 5.99 |
| 1.8 | 0.11 | 0.22 | 0.34 | 0.45 | 0.56 | 0.67 | 0.79 | 0.90 | 1.01 | 1.12 | 1.35 | 1.57 | 1.80 | 2.02 | 2.25 | 2.81 | 3.37 | 3.83 | 4.29 | 4.75 | 5.21 | 5.67 | 6.13 |
| 2.0 | 0.12 | 0.25 | 0.37 | 0.50 | 0.62 | 0.75 | 0.87 | 1.00 | 1.12 | 1.25 | 1.50 | 1.75 | 2.00 | 2.25 | 2.50 | 3.12 | 3.74 | 4.37 | 4.99 | 5.62 | 6.24 | 6.86 | 7.49 |
| 2.2 | 0.14 | 0.27 | 0.41 | 0.55 | 0.69 | 0.82 | 0.96 | 1.10 | 1.24 | 1.37 | 1.55 | 1.82 | 2.10 | 2.37 | 2.75 | 3.43 | 4.12 | 4.80 | 5.49 | 6.18 | 6.86 | 7.55 | 8.24 |
| 2.4 | 0.15 | 0.30 | 0.46 | 0.60 | 0.75 | 0.90 | 1.05 | 1.20 | 1.35 | 1.50 | 1.80 | 2.10 | 2.40 | 2.70 | 3.00 | 3.74 | 4.49 | 5.24 | 5.99 | 6.74 | 7.49 | 8.24 | 8.99 |
| 2.6 | 0.16 | 0.32 | 0.49 | 0.65 | 0.81 | 0.97 | 1.14 | 1.30 | 1.46 | 1.62 | 1.95 | 2.27 | 2.60 | 2.92 | 3.24 | 4.06 | 4.87 | 5.68 | 6.49 | 7.30 | 8.11 | 8.92 | 9.73 |
| 2.8 | 0.17 | 0.35 | 0.52 | 0.70 | 0.87 | 1.05 | 1.22 | 1.40 | 1.57 | 1.75 | 2.10 | 2.45 | 2.80 | 3.14 | 3.48 | 4.37 | 5.24 | 6.12 | 6.99 | 7.86 | 8.74 | 9.61 | 10.48 |
| 3.0 | 0.19 | 0.37 | 0.56 | 0.75 | 0.94 | 1.12 | 1.31 | 1.50 | 1.68 | 1.87 | 2.25 | 2.62 | 3.00 | 3.37 | 3.74 | 4.68 | 5.62 | 6.55 | 7.49 | 8.42 | 9.36 | 10.30 | 11.25 |
| 3.2 | 0.20 | 0.40 | 0.60 | 0.80 | 1.00 | 1.20 | 1.40 | 1.60 | 1.80 | 2.00 | 2.40 | 2.80 | 3.19 | 3.58 | 3.99 | 4.99 | 5.99 | 6.99 | 7.99 | 8.99 | 9.98 | 10.98 | 11.98 |
| 3.4 | 0.21 | 0.42 | 0.64 | 0.85 | 1.06 | 1.27 | 1.49 | 1.70 | 1.91 | 2.12 | 2.55 | 2.97 | 3.39 | 3.82 | 4.24 | 5.30 | 6.36 | 7.43 | 8.49 | 9.55 | 10.61 | 11.67 | 12.73 |
| 3.6 | 0.22 | 0.45 | 0.67 | 0.90 | 1.12 | 1.35 | 1.57 | 1.80 | 2.02 | 2.25 | 2.70 | 3.14 | 3.58 | 4.04 | 4.49 | 5.62 | 6.74 | 7.86 | 8.99 | 10.11 | 11.23 | 12.36 | 13.48 |
| 3.8 | 0.24 | 0.47 | 0.71 | 0.95 | 1.19 | 1.42 | 1.66 | 1.90 | 2.13 | 2.37 | 2.85 | 3.32 | 3.79 | 4.27 | 4.74 | 5.93 | 7.11 | 8.30 | 9.48 | 10.67 | 11.86 | 13.04 | 14.23 |
| 4.0 | 0.25 | 0.50 | 0.75 | 1.00 | 1.25 | 1.50 | 1.75 | 2.00 | 2.25 | 2.50 | 3.00 | 3.49 | 3.99 | 4.49 | 4.99 | 6.24 | 7.49 | 8.74 | 9.98 | 11.23 | 12.48 | 13.73 | 14.98 |
| 4.2 | 0.26 | 0.52 | 0.79 | 1.05 | 1.31 | 1.57 | 1.83 | 2.10 | 2.36 | 2.62 | 3.14 | 3.67 | 4.19 | 4.72 | 5.24 | 6.55 | 7.86 | 9.17 | 10.48 | 11.79 | 13.10 | 14.41 | 15.72 |
| 4.4 | 0.27 | 0.55 | 0.82 | 1.10 | 1.37 | 1.65 | 1.92 | 2.20 | 2.47 | 2.75 | 3.29 | 3.84 | 4.39 | 4.94 | 5.49 | 6.86 | 8.24 | 9.61 | 10.98 | 12.36 | 13.73 | 15.10 | 16.47 |
| 4.6 | 0.29 | 0.57 | 0.86 | 1.15 | 1.44 | 1.72 | 2.01 | 2.30 | 2.59 | 2.87 | 3.44 | 4.02 | 4.59 | 5.17 | 5.74 | 7.18 | 8.61 | 10.05 | 11.48 | 12.92 | 14.35 | 15.79 | 17.22 |
| 4.8 | 0.30 | 0.60 | 0.90 | 1.20 | 1.50 | 1.80 | 2.10 | 2.40 | 2.70 | 3.00 | 3.59 | 4.19 | 4.79 | 5.39 | 5.99 | 7.49 | 8.99 | 10.48 | 11.98 | 13.48 | 14.98 | 16.47 | 17.97 |
| 5.0 | 0.31 | 0.62 | 0.94 | 1.25 | 1.56 | 1.87 | 2.18 | 2.50 | 2.81 | 3.12 | 3.74 | 4.37 | 4.99 | 5.62 | 6.24 | 7.80 | 9.36 | 10.92 | 12.48 | 14.04 | 15.50 | 17.18 | 18.72 |
| 5.5 | 0.34 | 0.69 | 1.03 | 1.37 | 1.72 | 2.06 | 2.40 | 2.75 | 3.09 | 3.43 | 4.12 | 4.80 | 5.49 | 6.18 | 6.86 | 8.58 | 10.30 | 12.01 | 13.73 | 15.44 | 17.15 | 18.88 | 20.58 |
| 6.0 | 0.37 | 0.75 | 1.12 | 1.50 | 1.87 | 2.25 | 2.62 | 3.00 | 3.37 | 3.74 | 4.49 | 5.24 | 5.99 | 6.74 | 7.49 | 9.36 | 11.23 | 13.10 | 14.96 | 16.85 | 18.72 | 20.59 | 22.48 |
| 6.5 | 0.41 | 0.81 | 1.22 | 1.62 | 2.03 | 2.43 | 2.84 | 3.24 | 3.65 | 4.06 | 4.87 | 5.68 | 6.49 | 7.30 | 8.11 | 10.14 | 12.17 | 14.20 | 16.22 | 18.25 | 20.28 | 22.31 | 24.34 |
| 7.0 | 0.44 | 0.87 | 1.31 | 1.75 | 2.18 | 2.62 | 3.06 | 3.49 | 3.93 | 4.37 | 5.24 | 6.12 | 6.99 | 7.86 | 8.74 | 10.92 | 13.10 | 15.29 | 17.47 | 19.66 | 21.84 | 24.02 | 26.21 |

shear3.xls Shear A

R Chan Associates - Austin

Figure 9.35: Range of shear stresses allowable on slopes for different covers.

Source: Johnston (2003)

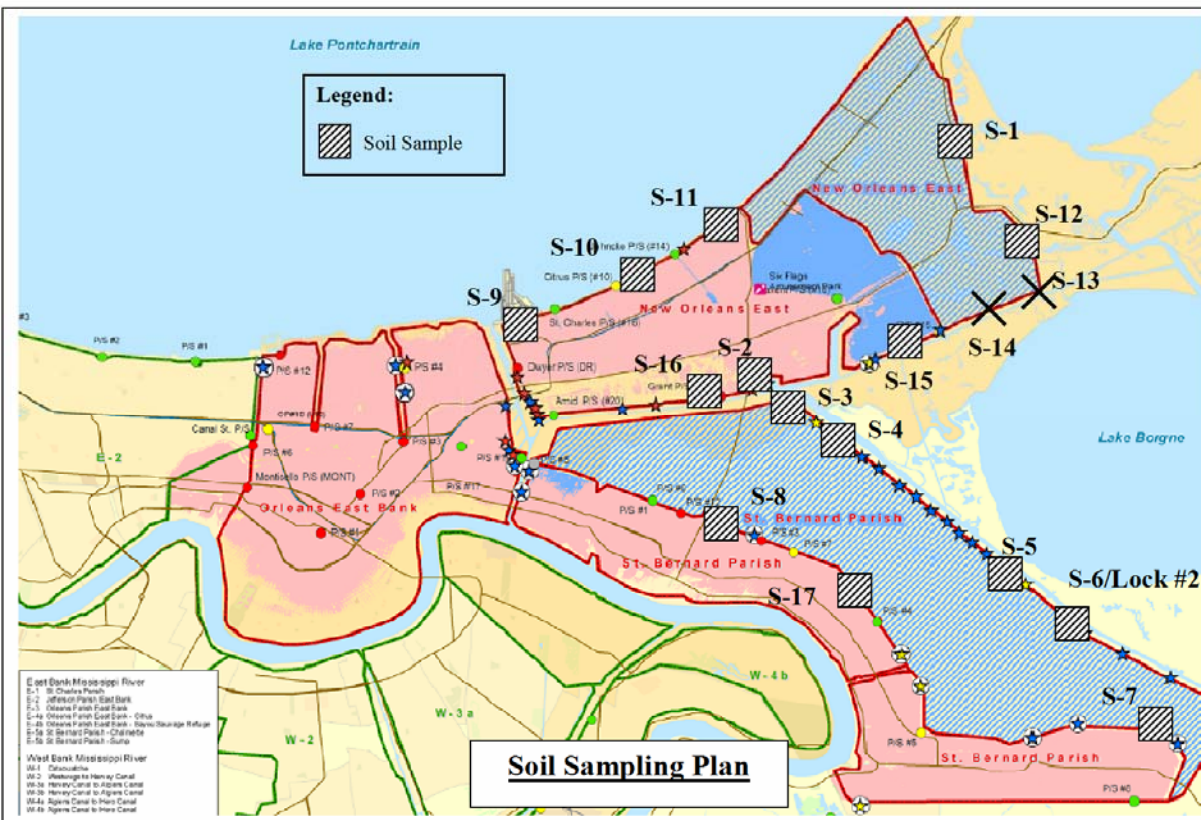


Figure 9.36: Location of samples.

Table 9.9: Salinity and pH of water associated with the samples

| | pH | Salinity (ppm) |
|-------------------|------|----------------|
| Sample S11 | 8.61 | 3287 |
| Sample S15 | 8.09 | 4199 |
| Typical sea water | 7.9 | 30000 to 35000 |
| Typical tap water | 7.0 | 500 |

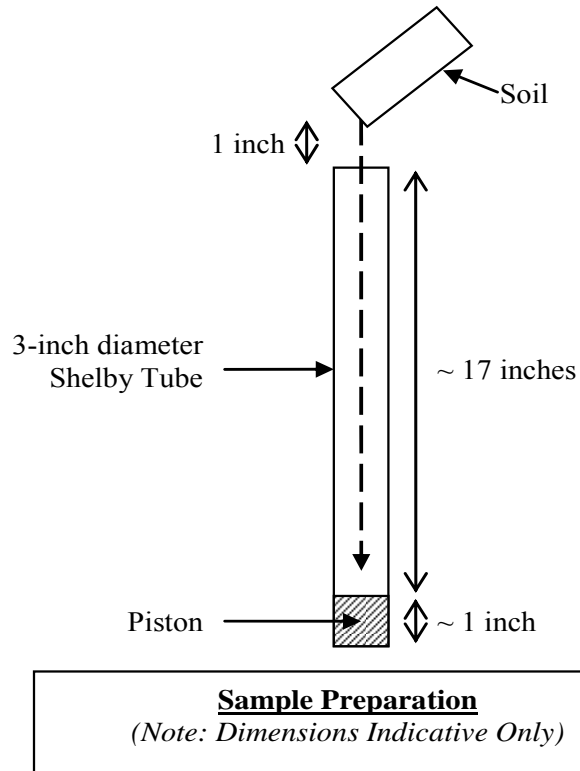


Figure 9.37: Soil preparation by re-compaction for bag samples.

EFA Test Results for Sample No. S4-(0-0.5ft)-LC-SW

Sample Type: Bulk Sample
Water Salinity: 36.1 PPT (Salt Water)
Compaction Effort: Low = 1.6% Modified Proctor Compaction

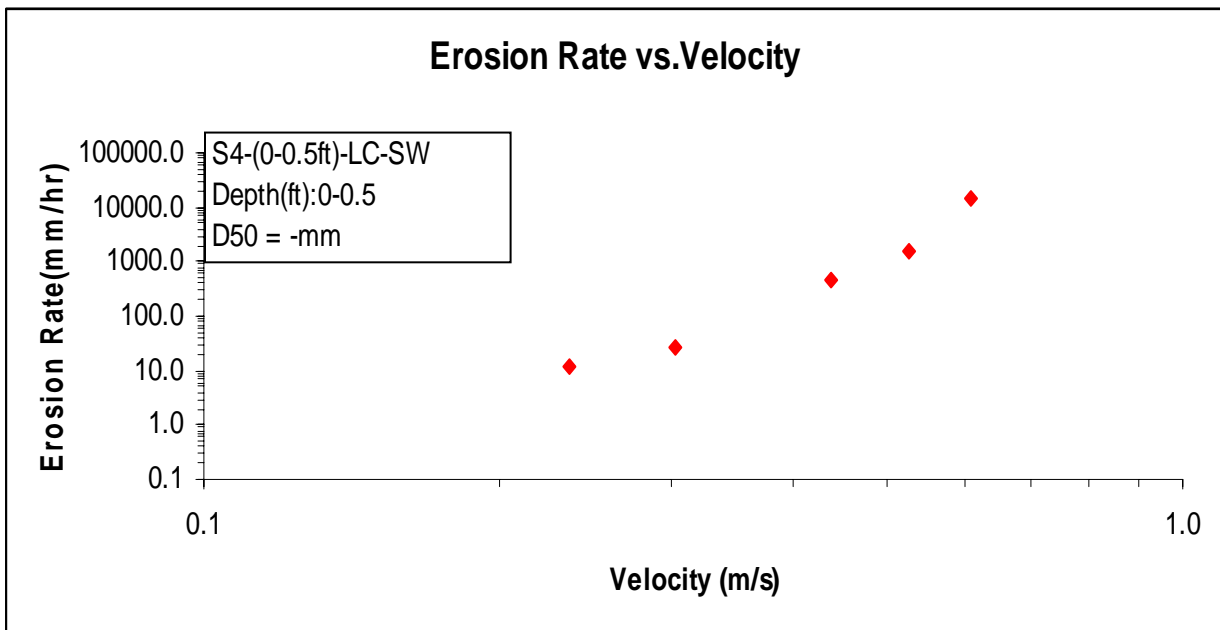
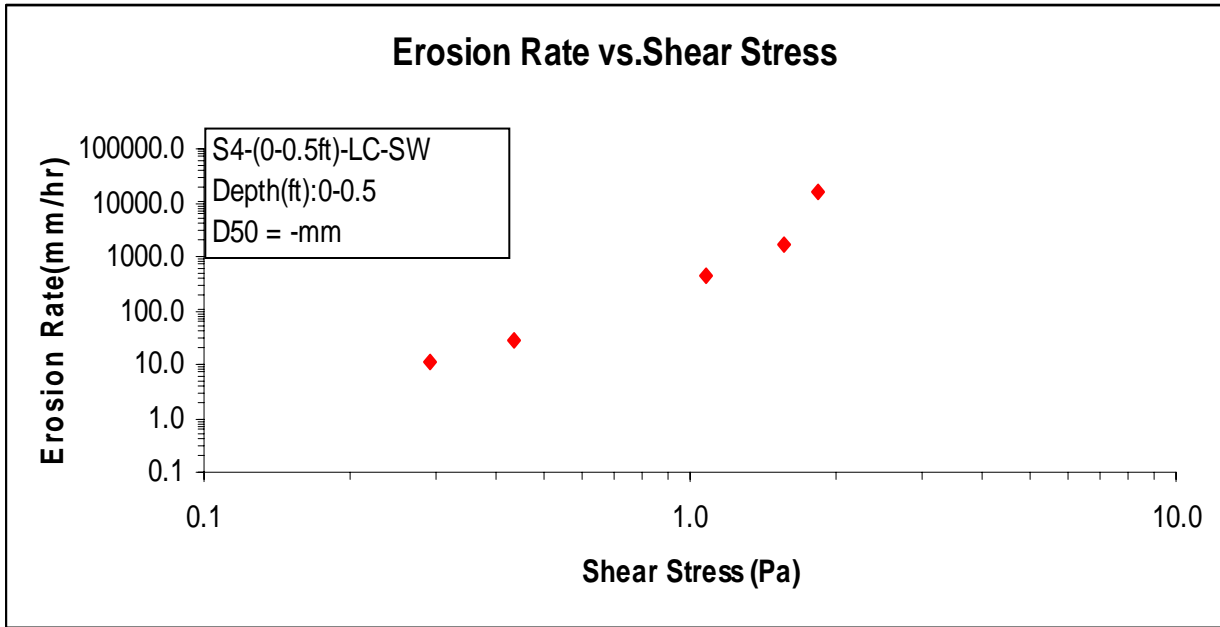


Figure 9.38: EFA test results for sample S4 (0-0.5 ft), low compaction, salt water.

EFA Test Results for Sample No. S3-B3-(0-1ft)-SW

Sample Type: Shelby Tube
Water Salinity: 36.4 PPT (Salt Water)
Compaction Effort: N/A

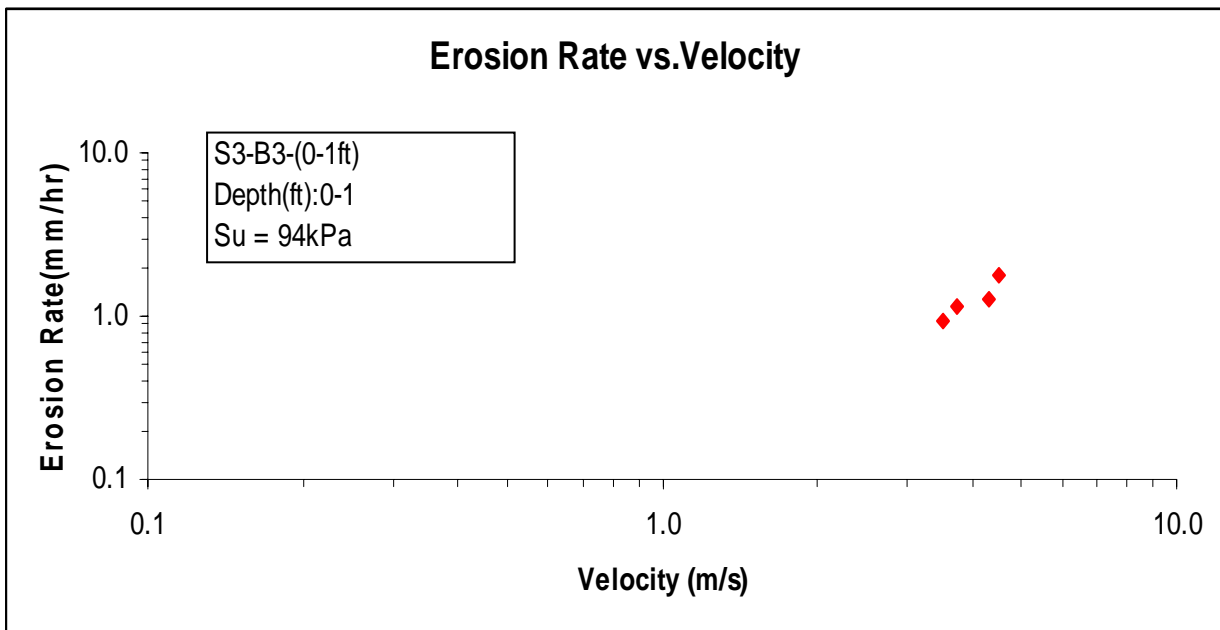
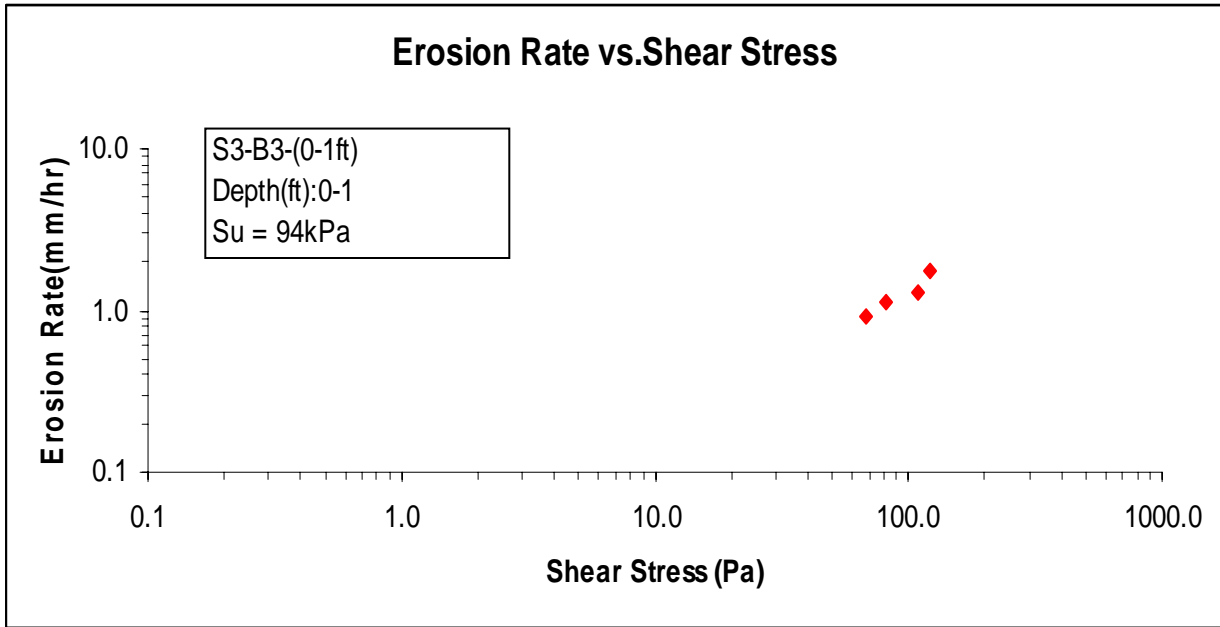


Figure 9.39: EFA test results for sample S3-B3 (0-1 ft), salt water.

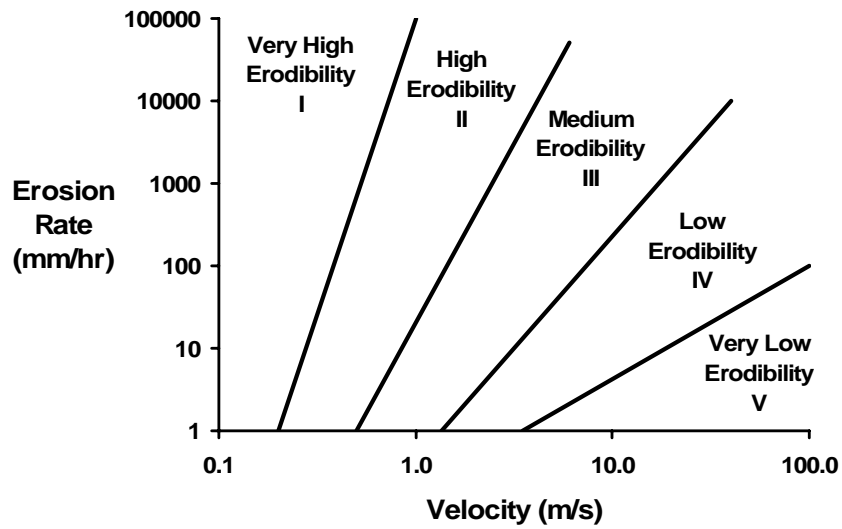


Figure 9.40: Erosion Chart.

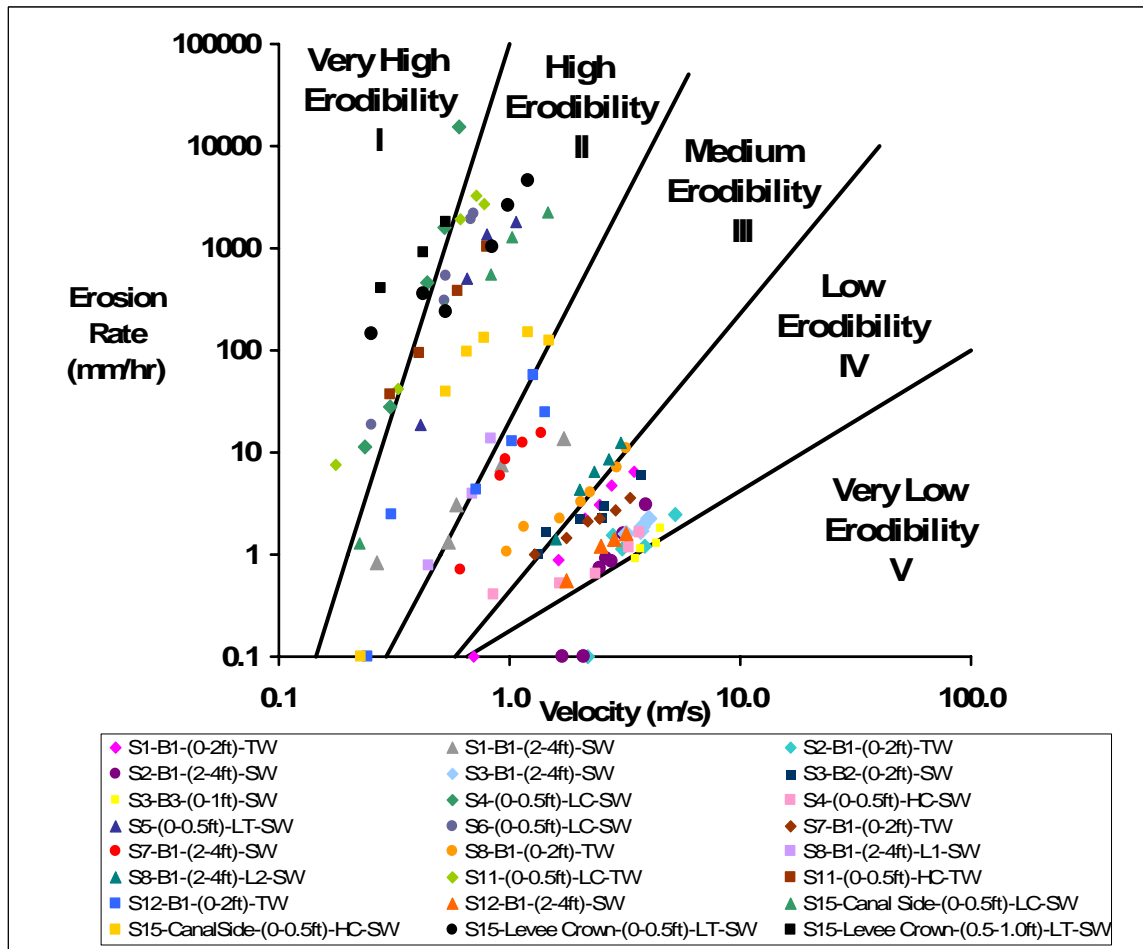


Figure 9.41: EFA test results for 24 levee samples.

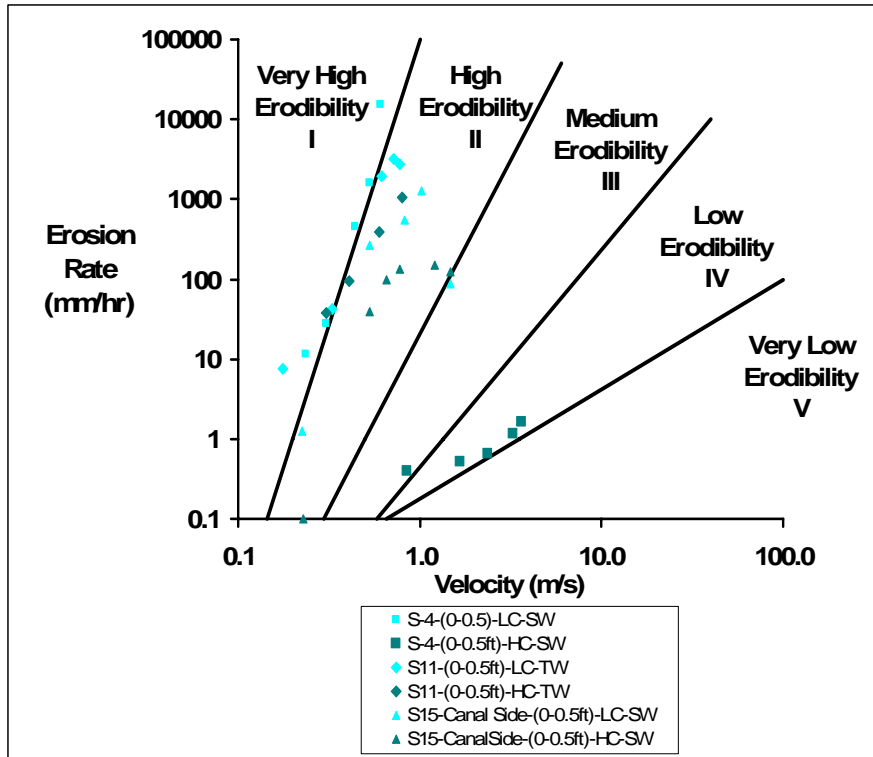


Figure 9.42: Influence of compaction on erodibility.

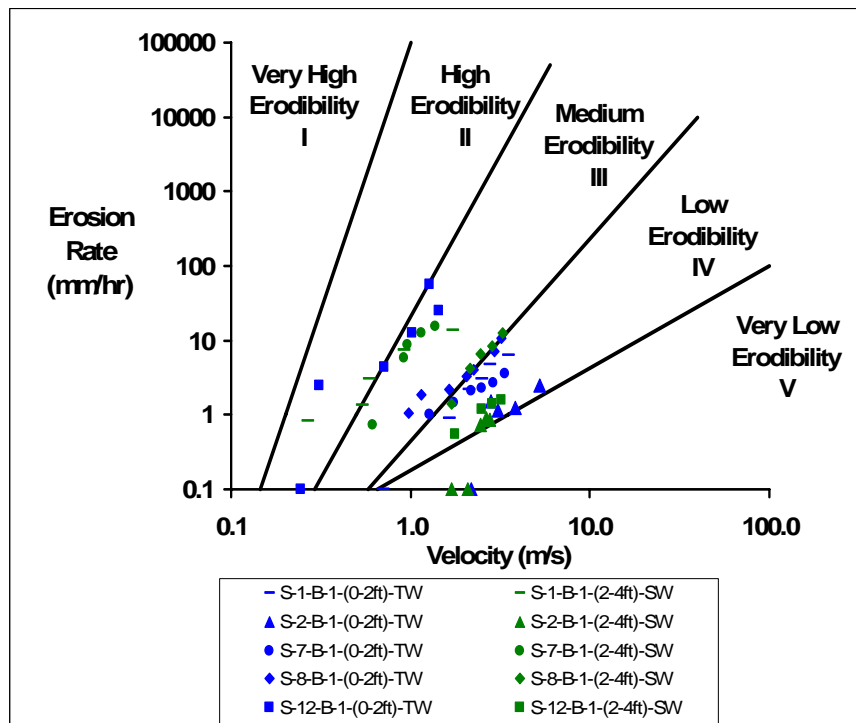


Figure 9.43: Influence of water salinity on erodibility.

Table 9.10: Results of the index property tests.

| Sample | Soil Description | Classification | γ_t (kN/m ³) | γ_{dry} (kN/m ³) | w (%) | Tested at Texas A&M University | | | | Tests Performed by STE | | | | |
|--------------------------------|---|----------------|------------------------------------|--|-------|--------------------------------|----|----|----|------------------------|---------|----|----|----|
| | | | | | | % fines | LL | PL | PI | Organic Content% | % fines | LL | PL | PI |
| S1-B1-(0-2ft)-TW | Clay with hard clay grain mixture | CH | 20.23 | 15.37 | 31.66 | - | 71 | 25 | 46 | 3.09 | 89.9 | 65 | 22 | 43 |
| S1-B1-(2-4ft)-SW | Clay with rootlets | CH | 19.10 | 15.69 | 21.77 | - | 56 | 19 | 37 | 1.91 | | | | |
| S2-B1-(0-2ft)-TW | Clay with rootlets | CL | 19.74 | 17.00 | 16.11 | - | 46 | 17 | 29 | 16.94 | 67.2 | 49 | 17 | 32 |
| S2-B1-(2-4ft)-SW | Clay | CL | 20.26 | 16.71 | 21.23 | 69.1 | 41 | 16 | 25 | 1.62 | | | | |
| S3-B1-(2-4ft)-SW | Clay | CL-CH | 17.60 | 13.86 | 27.00 | - | 48 | 17 | 31 | 2.50 | | | | |
| S3-B2-(0-2ft)-SW | Clay with some sand | CH | 20.20 | 17.26 | 31.66 | - | 69 | 23 | 46 | - | 90.3 | 54 | 19 | 35 |
| S3-B3-(0-1ft)-SW | Clay | CL-CH | 17.16 | 13.95 | 23.00 | - | 32 | 12 | 20 | 2.60 | | | | |
| S4-(0-0.5ft)-LC-SW | Clay with some sand | CL | 13.87 | 10.42 | 33.14 | 90.5 | 60 | 30 | 30 | 8.16 | - | - | - | - |
| S4-(0-0.5ft)-HC-SW | Clay with some sand | CL | 17.69 | 13.23 | 33.14 | | | | | | | | | |
| S5-(0-0.5ft)-LT-SW | Silt-Clay | | 21.85 | 18.15 | 20.40 | 54.4 | - | - | - | 0.69 | - | - | - | - |
| S6-(0-0.5ft)-LC-SW | Sand w/Some Clay | SP | 13.45 | 12.79 | 5.21 | 8.9 | - | - | - | 0.71 | - | - | - | - |
| S7-B1-(0-2ft)-TW | Clay | CH | 17.39 | 13.73 | 26.65 | - | 68 | 24 | 44 | 3.78 | 90.1 | 78 | 32 | 46 |
| S7-B1-(2-4ft)-SW | Clay with hard clay grain mixture | CH | 16.52 | 13.42 | 23.04 | - | - | - | - | 7.14 | | | | |
| S8-B1-(0-2ft)-TW | Clay with 1.5" thick grass on top of sample | CH | 17.71 | 13.38 | 32.34 | - | - | - | - | - | | | | |
| S8-B1-(2-4ft)-L1-SW | Clay with 2 layers | CH | 18.74 | 14.00 | 33.87 | - | - | - | - | 2.28 | | | | |
| S8-B1-(2-4ft)-L2-SW | Clay with 2 layers | CH | 18.74 | 14.00 | 33.87 | - | 54 | 21 | 33 | 15.37 | | | | |
| S11-(0-0.5ft)-LC-TW | Sand | SP | 12.30 | 12.23 | 1.02 | 0.1 | - | - | - | 0.32 | - | - | - | - |
| S11-(0-0.5ft)-HC-TW | Sand | SP | 13.26 | 13.12 | 1.02 | | - | - | - | 0.35 | - | - | - | - |
| S12-B1-(0-2ft)-TW | Clay with decomposed wood | CH | 14.77 | 10.19 | 44.94 | - | 67 | 27 | 40 | 16.91 | 92 | 67 | 21 | 46 |
| S12-B1-(2-4ft)-SW | Clay | MH-CH | 17.56 | 12.64 | 38.94 | - | 58 | 32 | 26 | 5.28 | | | | |
| S15-CanalSide-(0-0.5ft)-LC-SW | Sand w/Some Clay | | 13.85 | 12.21 | 13.43 | | - | - | - | 1.28 | | | | |
| S15-CanalSide-(0-0.5ft)-HC-SW | Sand w/some clay | SM | 19.63 | 17.31 | 13.43 | 29.9 | - | - | - | | | | | |
| S15-LeveeCrown-(0-0.5ft)-LT-SW | Sand w/Some Clay | | 13.29 | 11.94 | 11.29 | | - | - | - | 2.16 | | | | |
| S15-LeveeCrown-(0.5-1ft)-LT-SW | Sand w/Some Clay | | 13.57 | 12.46 | 8.93 | | - | - | - | 1.01 | | | | |

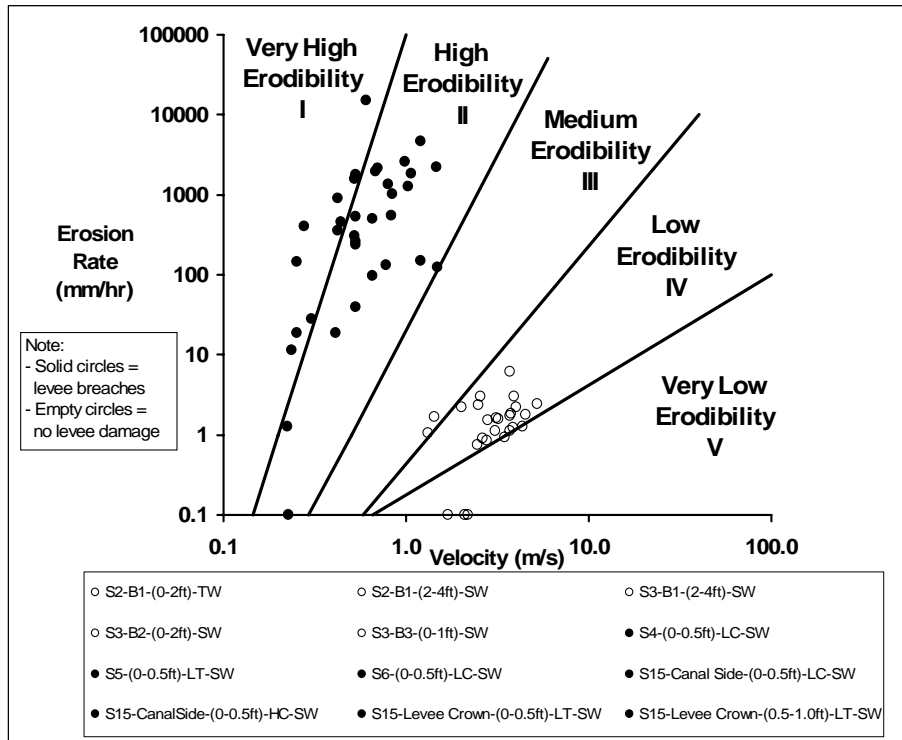


Figure 9.44: EFA test results and overtopping levee failure/no failure chart.

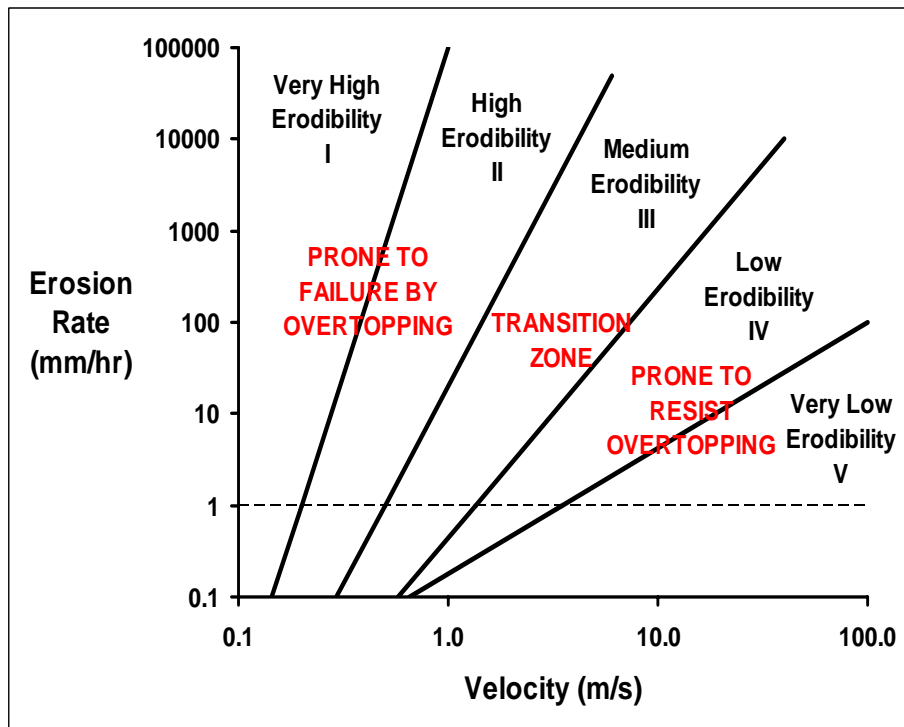


Figure 9.45: Proposed guidelines for levee overtopping.